Neutrophil-derived IL-17 limits protective host responses and promotes tuberculosis pathogenesis

Priya Sharma[1], Raman Deep Sharma[1], Mrinmoy Das[1], Binayak Sarkar[2], Lakshyaveer Singh[1], Neharika Jain[1], Shivam Chaturvedi[1], Lalita Mehra[3], Aditya Rathee[1], Shilpa Sharma[1], Shihui Foo[4], Andrea Lee[5], N Pavan kumar[6], Prasenjit Das[3], Vijay Viswanathan[7], Hardy Kornfeld[8], Shanshan W. Howland[4], Subash Babu[9,10], Vinay Nandicoori[2,11], Amit Singhal[5,12] and Dhiraj Kumar[1*]

[1]Cellular Immunology Group, International Centre for Genetic Engineering and Biotechnology, Aruna Asaf Ali Marg, New Delhi, India-110067
[2] National Institute of Immunology, Aruna Asaf Ali Marg, New Delhi, India-110067
[3]Department of Pathology, All India Institute of Medical Sciences, New Delhi, India-110012
[4]Singapore Immunology Network (SIgN), Agency for Science, Technology and Research (A*STAR), Singapore, Republic of Singapore.
[5]Infectious Diseases Labs (ID labs), Agency for Science, Technology and Research (A*STAR), Singapore, Republic of Singapore
[6]Department of Immunology, ICMR-National Institute for Research in Tuberculosis, Chennai, India – 600031
[7]Prof. M. Viswanathan Diabetes Research Center, Chennai, India
[8]Department of Medicine, University of Massachusetts Medical School, Worcester, MA, USA
[9]NIH-International Center of Excellence in Research, Chennai, India
[10]Laboratory of Parasitic Diseases, NIAID-NIH, Bethesda, Maryland, USA
[11]Centre for Cellular and Molecular Biology, Hyderabad, India
[12]Lee Kong Chian School of Medicine, Nanyang Technological University (NTU), Singapore, Republic of Singapore.

*Correspondence: dhiraj@icgeb.res.in

Running title: IL-17 and PMNs in Tuberculosis Pathogenesis

Abstract

The protective correlates of *Mycobacterium tuberculosis* (*Mtb*) infection-elicited host immune responses are incompletely understood. Here we report pro-pathogenic crosstalk between IL-17, COX2, and Neutrophils. We show that most intracellular bacilli in the wild-type (WT) mice's lungs are neutrophil-resident. In BCG-vaccinated WT mice, *Mtb* continues to persist inside neutrophils, which is sensitive to COX2 inhibition. Using a genetically susceptible *IFNγ*$^{-/-}$ mice model, we report that excessive neutrophil infiltration and corresponding bacteremia are dependent on neutrophil-derived IL-17. COX2 inhibition and IL-17 neutralization reverse neutrophil infiltration, associated pathology and death in *IFNγ*$^{-/-}$ mice. The IL-17-Neutrophils interplay also operates in WT mice, and RORγt inhibition enhances BCG's protective efficacy. In a prospective clinical cohort of pulmonary TB, high neutrophil count and IL-17 precipitate adverse treatment outcomes. We propose targeting the pro-pathogenic IL-17- Neutrophils axis to enhance TB prevention and therapy in normal and vulnerable subjects.

48 **Introduction**

49 Tuberculosis (TB) is the major cause of mortality and morbidity due to an infectious disease.
50 A lack of an effective vaccine, prognostic diversity among the patients, and the emergence of
51 drug resistance greatly hamper the efforts to control TB. BCG, the only available vaccine, has
52 limited efficacy in adults, although it works well in preventing childhood TB and TB
53 meningitis. A comprehensive understanding of how the host immune system responds to
54 vaccination, infection and treatment is fundamental to the success of TB elimination
55 programs (Chandra et al., 2022). Not all individuals exposed to *Mtb* follow a common
56 trajectory on parameters like developing latent or active disease, disease severity and
57 responsiveness to anti-TB chemotherapy (Barry et al., 2009; Cadena et al., 2017; Dartois and
58 Rubin, 2022; Heyckendorf et al., 2021; Pai et al., 2016; Thompson et al., 2017). For example,
59 the average treatment success rate for TB is ~80%, which is further lower in the case of drug-
60 resistant TB (DR-TB, 50%) (Chaves Torres et al., 2019; Rockwood et al., 2016).
61 Immunological features that contribute to treatment success and failure in non-DR-TB
62 patients, presents a unique opportunity to understand the host immunity associated with
63 protection against TB. Unfortunately, the immune parameters that define vaccine efficacy or
64 treatment outcomes are poorly understood. There is a consensus that host-driven mechanisms
65 play a critical role in the differential BCG response between young children and adults
66 (Brazier and McShane, 2020). For example, the BCG-induced memory T-cell responses are
67 believed to fade over time (Soares et al., 2013). For intracellular pathogens like *Mtb*,
68 understandably, the cell-mediated immunity arm acquires greater importance in terms of
69 vaccine efficacy (Brazier and McShane, 2020). However, since the bacteria mostly reside
70 inside the innate immune cells, it is pertinent to ask- whether innate immune-based
71 mechanisms also contribute to the differential protective responses. To further elaborate, the
72 presence of *Mtb* has been shown in unconventional cells like mesenchymal stem cells

73 (MSCs), bone cells, adipocytes etc. (Das et al., 2013; Fatima et al., 2020; Jain et al., 2020).
74 The bacteria residing in the MSCs can escape immune cytokines like IFNγ and TNFα, which
75 could effectively blunt the T-cell-mediated protective immune responses (Jain et al., 2020).
76 TB granulomas also comprise other innate immune cells, like granulocytes and dendritic cells
77 (Cadena et al., 2017). Whether different cellular constituents confound the protective host
78 responses remains poorly understood. Neutrophils are the most extensively studied
79 granulocytes in the context of TB (Dallenga and Schaible, 2016; Kimmey et al., 2015;
80 Lovewell et al., 2021; Mishra et al., 2017). They represent the most common *Mtb*-containing
81 innate cells in the airways of active TB patients (Eum et al., 2010). Recent studies point to a
82 more pathological role of neutrophils in TB (Berry et al., 2010; Han et al., 2018; Lowe et al.,
83 2013; Nwongbouwoh Muefong et al., 2022) although some studies also report their protective
84 roles in specific contexts (Lowe et al., 2018; Martineau et al., 2007; Silva et al., 1989).
85 Using the mice model of tuberculosis, we explored neutrophils as a distinctive and preferred
86 niche for *Mtb* in this study. Our results show that neutrophil-resident *Mtb* contributes to lower
87 the efficacy of BCG vaccines and precipitates incidences of severe pathology and treatment
88 failure. We propose targeting this population can significantly enhance the preventive
89 responses of BCG, enable better control in genetically vulnerable subjects, and provide an
90 unexpected opportunity for host-directed therapy against TB.

91 **Results**

92 **Neutrophils serve as the major niche for *Mycobacterium tuberculosis* in mice lungs.**

93 To assess diverse cellular niches in the lungs of *Mtb*-infected C57BL/6 (WT) mice, we
94 investigated intracellular burden in Ly6G$^+$ CD11b$^+$ neutrophils (herein after also referred as
95 polymorphonuclear neutrophils or PMNs), CD64$^+$MerTK$^+$ macrophages and
96 Sca1$^+$CD90.1$^+$CD73$^+$ mesenchymal stem cells (MSCs). Mice were infected with 100-200
97 H37Rv colony forming units (CFUs) via aerosol challenge, and at 4, 8 and, 12 weeks post-
98 infection (p.i.), the total bacterial burden in the lung and spleen was estimated by CFU
99 counting (Fig. S1A-C). Half of the lungs from each animal was processed to flow-sort PMNs,
100 Macrophages and MSCs following the gating strategy shown in Fig. S1D. Among the three
101 cell populations, MSCs were the most abundant cell type across each of the time points post
102 *Mtb* infection (2-6x10^4/million sorted cells), followed by macrophages (4-9x10^3/million
103 sorted cells) and PMNs (1-4x10^3 /million sorted cells, Fig. S1E). However, PMNs contained,
104 on an average, 4-5 times more total bacillary load (from the total sorted pool of cells) as
105 compared to either macrophages or MSCs (Fig. S1F). To account for the differences in the
106 total number of the three cell types, we calculated CFU/10^4 cells. This also showed the
107 highest bacillary load in the PMNs (Fig. S1G). Thus, a disproportionately large number of
108 *Mtb* in the lungs of infected animals reside inside the PMNs, which outnumber those present
109 in macrophages or MSCs.

110 **The residual *Mtb* population in BCG-vaccinated animals are largely neutrophil-**
111 **resident.**

112 To understand the relevance of neutrophil-resident *Mtb* and its contribution towards TB
113 pathogenesis, we repeated the above experiments in BCG-vaccinated animals. Mice were
114 administered either PBS or BCG (Pasteur strain) intradermally, followed by aerosol challenge
115 with H37Rv at eight weeks post-BCG vaccination (Fig. 1A). As expected, animals that

116 received BCG showed nearly ten-fold lower bacterial burden in the lungs and spleen
117 compared to the unvaccinated PBS controls (Fig. 1B-C). Consequently, BCG-vaccinated
118 animals also showed less pathology as compared to the unvaccinated PBS controls (Fig.
119 S1H). Among the sorted cells from the lungs, except for a marginal decline in PMNs number
120 at eight weeks post-infection in the BCG-vaccinated group, the relative distribution of PMNs,
121 macrophages and MSCs in both control and BCG-vaccinated animals remained unperturbed
122 over the course of infection (Fig. 1D). The bacterial burden, however, in each of the three cell
123 types dropped significantly (by 80-90%) in the BCG-vaccinated animals (Fig. 1E). Curiously,
124 lung PMNs in BCG-vaccinated mice still contained 10-20-fold more bacilli compared to the
125 other two cell types for each time points p.i. investigated (Fig. 1E). These results indicate that
126 BCG-induced protective host immunity is unable to control the PMNs -resident *Mtb*
127 efficiently. Thus, it appears that PMNs serve as a protective niche for *Mtb* against
128 immunological assaults such as BCG vaccination in mice.

129 **RNAseq analysis of neutrophils sorted from the lungs of infected animals.**

130 We next analyzed the global gene expression profile of flow-sorted PMNs from the lungs of
131 unvaccinated or BCG-vaccinated mice, either uninfected or *Mtb*-challenged (Fig. 1F). Only
132 27 differentially regulated genes were found between unvaccinated, uninfected (UI) and
133 BCG-vaccinated, uninfected animals, and therefore, the BCG-vaccinated, uninfected mice
134 group was excluded from the heatmap in figure 1F (Table S1). Compared to the UI control
135 group, 944 genes were differentially expressed in the *Mtb*-infection group alone, whereas
136 there were 620 DEGs in the BCG-vaccinated *Mtb*-infected group, 373 genes being common
137 to both the lists (Fig. S1I). Compared to the *Mtb*-infected group, the BCG-vaccinated *Mtb*-
138 infected group had 209 DEGs (Fig. S1I). The union of these DEGs (n=1332) formed seven
139 distinct clusters (Fig. 1F, Table S2). Table S2 shows Gene Ontology Biological Process (GO-
140 BP) enriched among genes in each cluster. Clusters 2 and 6 comprised of downregulation and

141 upregulation, respectively, upon *Mtb* infection alone, the expression of which were not
142 altered by BCG-vaccination (Fig. 1F). For the remaining five clusters, a few selected GO-BP
143 classes and corresponding genes are shown in figure 1F. Each of these clusters showed a
144 distinctive pattern in the BCG-vaccinated group compared to the *Mtb*-infected group.
145 Compared to the unvaccinated *Mtb*-infected group the expression of genes for clusters 1 and
146 3 was reverted in the BCG-vaccinated *Mtb*-infected group to the level observed in uninfected
147 animals, suggesting BCG vaccination-mediated reversal in the neutrophil transcriptional
148 program. The cluster 1 genes (upregulated in BCG-vaccinated *Mtb*-infected group) belonged
149 to functional classes like xenophagy, T cell proliferation, Eosinophil activation etc., whereas
150 genes in cluster 3 (downregulated in BCG-vaccinated-*Mtb*-infected group) were involved in
151 lactate metabolism, mitophagy, microtubule polymerization etc. Similarly, genes in cluster 4
152 (downregulated in BCG-vaccinated-*Mtb*-infected group) belonged to functional classes like
153 blood vessel remodelling, inflammatory response to wounding, TGFβ signalling and Th17
154 cell chemotaxis (Fig. 1F). Th17 cell chemotaxis has been associated with exacerbated TB
155 pathology and therefore a decline in this pathway in BCG-vaccinated group concurred with
156 earlier studies(Jung et al., 2022) (Basile et al., 2011; Jurado et al., 2012; Mills, 2023). Genes
157 in cluster 5 were upregulated only in the BCG-vaccinated-*Mtb*-infected group and belonged
158 to steroid metabolism, TLR2 signaling pathway, epithelium cell activation and leukotriene
159 production (Fig. 1F). To note, increased production of leukotriene is also associated with TB
160 protection (Pavan Kumar et al., 2019; Peres et al., 2007; Tobin et al., 2010). Cluster 7 genes,
161 expression of which was marginally lower in the BCG-vaccinated *Mtb*-infected group
162 compared to the *Mtb*-infected group alone, belonged to IL1β production, response to type I
163 IFN, macrophage activation and nitric oxide production (Fig. 1F). Taken together, RNAseq
164 analysis provided insights into the association of the functional states of PMNs with either
165 pathology (*Mtb*-infected) or protection (BCG-vaccinated, *Mtb*-infected) from TB.

166 **Celecoxib potentiates the effect of BCG by targeting the neutrophil-resident bacterial**
167 **population.**
168 The RNAseq data indicated an association of enhanced leukotriene pathway with the
169 protective functional state of neutrophils in the BCG-vaccinated *Mtb*-infected group (cluster
170 5, Fig. 1F). Neutrophil recruitment to the site of inflammation is driven by the chemotactic
171 signaling via receptor CXCR2 (Kolaczkowska and Kubes, 2013) and the eicosanoids
172 downstream to COX2 (Funk, 2001; Lemos et al., 2009). The COX2 enzyme competes with 5-
173 lipoxygenase (5-LO) enzyme for the substrate arachidonic acid to promote prostaglandin and
174 thromboxane biosynthesis (Funk, 2001). On the other hand, 5-LO promotes leukotriene
175 synthesis pathways. We found increased prostaglandin E2 (PGE2) level in the lung
176 homogenates of *Mtb*-infected mice compared to the uninfected mice (Fig. S2A). Since BCG
177 vaccination was associated with the activation of leukotriene pathway (Fig. 1F), we
178 hypothesized that skewing the balance away from PGE2 biosynthesis may impact the
179 survival of neutrophil-resident *Mtb* pool. Therefore, we treated unvaccinated and BCG-
180 vaccinated *Mtb*-infected mice with celecoxib, a specific COX2 inhibitor, and evaluated total
181 lung and spleen CFU at 8- and 12-week p.i. and PMNs-resident *Mtb* pool in the lungs at 12-
182 week p.i. (Fig. 2A). Celecoxib (50mg/kg/day) significantly reduced the bacterial burden in
183 the lungs of unvaccinated and BCG-vaccinated *Mtb*-infected mice, with a greater impact in
184 BCG-vaccinated mice (Fig. 2B). While the responses were similar in both lungs and spleen,
185 they were more pronounced in the lungs (Fig. 2B). This corresponded to celecoxib-mediated
186 decline in PMNs-resident pool of *Mtb* (by ~45%) in the lung of BCG-vaccinated *Mtb*-
187 infected mice (Fig. 2C). To note, celecoxib treatment had no significant effect on the
188 bacterial burden in macrophages and MSCs (Fig. 2C). Furthermore, histological analysis
189 revealed significant recovery in the lung pathology in BCG-vaccinated animals that received
190 celecoxib (Fig. 2D). Finally, neither BCG or celecoxib treatment had any significant impact

191 on the number of PMNs, macrophages or MSCs in the lungs at 12 weeks p.i. (Fig. S2B).
192 These results suggest a role of COX2 in determining the intracellular *Mtb* pool in the
193 neutrophils.
194 To assess the effect of celecoxib on the transcriptional landscape of neutrophils, we
195 performed RNAseq on sorted lung PMNs from celecoxib-treated unvaccinated or BCG-
196 vaccinated *Mtb*-infected mice. Here we compared the transcriptome of PMNs from
197 uninfected mice with those from *Mtb*-infected, celecoxib-treated *Mtb*-infected and celecoxib-
198 treated, BCG-vaccinated and *Mtb*-infected mice (Fig. 2E, Table S3). A total of 2190 genes
199 were differentially regulated in this comparison group, which could be clustered in four major
200 clusters (Fig. 2E, Table S3). Cluster 2 was of particular interest since it was majorly
201 upregulated only in the group that was BCG-vaccinated, *Mtb*-infected and received celecoxib
202 (Fig. 2E). Functionally, these genes belonged to biological processes like wound healing,
203 muscle tissue development, phagocytosis, mononuclear cell proliferation and differentiation
204 (Fig. 2F, Table S3). To understand the direct targets of celecoxib in the PMNs, we compared
205 genes from celecoxib-treated and *Mtb*-infected mice with those from celecoxib-treated, BCG-
206 vaccinated and *Mtb*-infected mice. Of around 23 common genes, a majority of them belonged
207 to defence mechanisms like response to IFNγ, TNF, LPS and production of cytokines in
208 inflammatory response (Fig S2C, Table S4). It, therefore, appears that celecoxib activates
209 anti-bacterial effector function in the neutrophils of *Mtb*-infected mice. These results
210 underscore two important points- i) PMN's effector functions appear to be perturbed during
211 *Mtb* infection, and ii) inhibiting COX2 triggers anti-bacterial pathways in the PMNs.
212 **In the *IFNγ*$^{-/-}$ animals, neutrophils account for high bacterial burden and disease**
213 **pathology.**
214 The results so far demonstrate a key role of PMNs-resident *Mtb* in TB pathology. While
215 COX2 inhibition helped clear this pool of *Mtb*, the mechanism of PMNs-driven pathology

216 was unclear. To understand the mechanism, we used *IFNγ*$^{-/-}$ animals, which are known to
217 develop severe neutrophilia and pathology upon *Mtb* infection (Cooper et al., 1993; Flynn et
218 al., 1993; Pearl et al., 2001). We first confirmed the severe disease phenotype in *Mtb*-infected
219 *IFNγ*$^{-/-}$ mice (Fig. 3A), which included severe gross pathology in the lungs, a very high
220 bacterial burden in the lungs and spleen and high mortality, compared to WT mice (Fig. S3A-
221 C). Histopathology analysis of lung sections revealed massive infiltration of the immune cells
222 (Fig. 3B), especially PMNs, as shown by immunofluorescence staining in the *IFNγ*$^{-/-}$ mice
223 compared to the WT mice (Fig. 3C). *Mtb*-infected *IFNγ*$^{-/-}$ mice showed a nearly 40-fold
224 higher number of PMNs (Fig. 3D) and ~2.5-fold higher macrophage numbers than the WT
225 animals (Fig. S3D). Unlike PMNsand macrophages, a decline in the number of MSCs was
226 observed in *IFNγ*$^{-/-}$ mice than the WT animals (Fig. S3D). In terms of resident *Mtb* in the
227 sorted cells, bacterial burden increased several folds in each of the three cell types (Fig. 3E
228 and S3E). However, due to the sheer number, there were more bacteria in the PMN
229 compartment than any other cell types in the *IFNγ*$^{-/-}$ mice, especially at 10 weeks p.i. Thus,
230 massive infiltration of PMNs and a very high intracellular *Mtb* burden in PMNs signifies
231 severe pathology in *IFNγ*$^{-/-}$ mice.

232 **Cytokine dysregulation in *IFNγ*$^{-/-}$ animals suggests a role of IL17 in disease pathology.**
233 To understand what contributed to the increased immune cells infiltration in the *Mtb*-infected
234 *IFNγ*$^{-/-}$ animals, we analyzed cytokine levels in the lung homogenates of the infected mice.
235 Several cytokines/chemokines were significantly dysregulated in the *Mtb*-infected *IFNγ*$^{-/-}$
236 mice compared to the *Mtb*-infected WT mice (Fig. 3F-G, S3G). Among those CXCL1,
237 CXCL2, IL-1β, IL-1α, IL-6, IL-17A (broadly known as IL-17), M-CSF, CCL3 and TNFα
238 were significantly upregulated (Fig. 3F) whereas IFNγ, IL-12, IL-9, IL-10, IL-15, IL-18, IL-
239 27 and IL-28 were downregulated (Fig. 3G). Among the upregulated cytokines in *Mtb*-

240 infected *IFNγ*$^{-/-}$ animals, CXCL1 and CXCL2 are the known chemoattractant for the PMNs
241 recruitment (Kolaczkowska and Kubes, 2013), whereas IL-1α, IL-1β and IL-6 are key
242 players in differentiation and expansion of the Th17 cells (Ketelut-Carneiro et al., 2019; Lee
243 et al., 2010; Mills, 2023). Interestingly, IL-17 was also significantly upregulated in the *Mtb*-
244 infected *IFNγ*$^{-/-}$ animals (Fig. 3F). Thus, more than one cytokine increased in the lungs of
245 *IFNγ*$^{-/-}$ animals upon *Mtb* infection converged to IL-17 regulation, indicating a key role for
246 IL-17 in disease pathology, which also concurs with earlier studies (Cruz et al., 2010).

247 **Neutrophils are the key source of IL-17 in TB granulomas**

248 IL-17 is a classical pro-inflammatory cytokine predominantly secreted by the Th_{17} cells,
249 which are important for TB pathology (Mills, 2023). Also, IL-17 has been shown to be
250 responsible for the recruitment and activation of neutrophils (Allen et al., 2015). To
251 investigate the source of IL-17, we first analyzed the IL-17-producing cells in the lungs of
252 *Mtb*-infected WT mice (Fig. 4A). To our surprise, >80% of PMNs were also positive for IL-
253 17 in the lungs of *Mtb*-infected WT mice (Fig. 4A). In the $CD45^{+}CD11b^{-}Ly6G^{-}$ population,
254 which mostly represented adaptive immune cells like T cells, B cells, NK cells etc., ~48%
255 were also positive for IL-17 (Fig. 4A). Immuno-fluorescence analysis of lung sections from
256 *Mtb*-infected WT mice revealed similar observation when stained for CD4 and IL-17. While
257 we could witness CD4 and IL-17 co-expressing cells, several IL-17^{+} cells lacked CD4
258 expression (Fig. 4B). Staining for Ly6G and IL-17 revealed intense IL-17-Ly6G co-staining
259 in the lung tissue sections of *Mtb*-infected WT mice, suggesting PMNs as the source of lung
260 IL-17 (Fig. 4C). A similar IL-17-Ly6G co-staining was also observed in the *Mtb*-infected
261 *IFNγ*$^{-/-}$ mice (Fig. 4D). Interestingly, even in human TB granulomas, we observed significant
262 co-staining of CD66b (the human neutrophil marker) and IL-17 (Fig. 4E). Thus, it appears
263 that there is an IL-17-PMNs axis operational during *Mtb* infection, which may contribute
264 towards TB pathology.

265 **IL-17 neutralization controls bacterial burden and disease pathology in *IFNγ*$^{-/-}$ animals**

266 The impact of IL-17 on TB pathogenesis is not unequivocally established. For example, IL-
267 17 is believed to exacerbate TB pathology during the chronic phase of infection, partly
268 through excessive neutrophil recruitment (Torrado and Cooper, 2010). On the other hand, a
269 more protective role of IL-17 in the WT mice was reported when infected with a
270 hypervirulent strain of *Mtb* (Domingo-Gonzalez et al., 2017). Since the results in the above
271 sections suggested a pro-pathogenic role of IL-17, we decided to neutralize IL-17 in *Mtb*-
272 infected *IFNγ*$^{-/-}$ mice. The *Mtb*-infected *IFNγ*$^{-/-}$ mice were administered anti-IL-17
273 monoclonal Ab (mAb) intra-peritoneally every 3-4 days, starting a day before the infection
274 (Fig. 5A). Similar to the WT mice, the lung homogenates of *IFNγ*$^{-/-}$ mice also showed a
275 copious amount of PGE2 upon *Mtb* infection, prompting us to include a celecoxib arm in this
276 experiment (Fig. S4A, Fig. 5). A significant decline in IL-17 levels in the lung homogenates
277 was observed in IL-17 mAb-administered mice (Fig. S4B). Neutralizing IL-17 led to a
278 significant decline in the number of infiltrating PMNs in the lungs of *Mtb*-infected *IFNγ*$^{-/-}$
279 mice (Fig. 5B). Unlike PMNs, there was no effect of IL-17 neutralization on the number of
280 macrophages or MSCs (Fig. S4C). *Mtb*-infected *IFNγ*$^{-/-}$ mice that received celecoxib alone
281 also showed a significant decline in PMN recruitment (Fig. 5B). There was no additive effect
282 on the recruitment of PMNs when celecoxib treatment was given in addition to IL-17 mAb
283 (Fig. 5B). While IL-17 neutralization alone reduced PMN recruitment, it could not bring
284 down the *Mtb* burden in the lungs of *IFNγ*$^{-/-}$ mice (Fig. 5C). Combined with celecoxib, IL-17
285 neutralization significantly brought down the *Mtb* burden in the lungs of *IFNγ*$^{-/-}$ mice (Fig.
286 5C). Unlike in the lungs, IL-17 neutralization alone was sufficient to reduce bacterial
287 dissemination to the spleen (Fig. 5D), suggesting PMN's active role in *Mtb* dissemination.
288 Moreover, IL-17 neutralization or celecoxib treatment alone did not impact bacterial burden
289 in the sorted lung PMNs (Fig. 5E). However, the combination of IL-17 neutralization and

290 celecoxib treatment significantly brought down bacterial load in the PMNs (Fig. 5E). On the
291 contrary, celecoxib alone significantly reduced the bacterial burden in the sorted
292 macrophages and the MSCs (Fig. S4D). Combined with IL-17 neutralization, macrophage-
293 resident but not MSC-resident *Mtb* numbers further declined compared to celecoxib treatment
294 alone (Fig. S4D). Accordingly, IL-17 neutralization alone or in combination with celecoxib
295 treatment led to a significant rescue in the survival of *IFNγ*$^{-/-}$ animals (Fig. 5F) and recovery
296 in lung pathology (Fig. 5G-H). Taken together, while celecoxib alone is insufficient to
297 control bacterial burden in *IFNγ*$^{-/-}$ animals, combined with IL-17 neutralization, it effectively
298 controls *Mtb* growth, tissue pathology and dissemination.

299 **Pathological role of PMN-derived IL-17 in the lungs of *Mtb*-infected *IFNγ*$^{-/-}$ animals.**

300 To check the effect of IL-17 neutralization or celecoxib treatment on local IL-17-producing
301 cells, we first assessed the number of IL-17-positive T helper cells (Th_{17}) in the single-cell
302 preparations from the lungs. While there was a trend of a decline in the number of Th_{17} cells
303 upon either IL-17 neutralization alone or in combination to COX2 inhibition in the lungs of
304 *Mtb*-infected *IFNγ*$^{-/-}$ mice, those changes were not found significant (Fig. 5I). In the lung
305 sections stained for IL-17 along with Ly6G, IL-17 neutralization, either alone or in
306 combination with COX2 inhibition, led to a consistent decline in IL-17^{+} Ly6G^{+} cells (Fig.
307 5J). The results from IL-17 ELISA in the lung homogenates, Th_{17} cell count in the lungs and
308 IL-17-Ly6G co-staining together suggest that while IL-17 contributes to high PMN
309 infiltration, PMNs itself are a significant source of IL-17, thereby establishing a vicious loop.
310 Since PMNs are also known to express IL-17 receptors (Tan et al., 2013; Taylor et al., 2014),
311 these results raise the possibility that IL-17 and PMNs could establish a self-amplification
312 loop, leading to severe TB pathology.

313 **Two distinct populations of PMNs with contrasting behaviours determine the fate of**
314 **infection.**

315 Both pro- and anti-bacterial roles are attributed to PMNs largely due to some heterogeneity in
316 the PMN population (Leliefeld et al., 2018; Tsuda et al., 2004). Results in earlier sections
317 showed a non-linear association between PMN numbers, associated bacterial burden and
318 overall bacteremia in the lung. For example, BCG or BCG and celecoxib did not reduce PMN
319 numbers, but the PMN-resident bacterial pool and total tissue bacterial load showed a
320 significant decline (Fig. 2). On the other hand, in *IFNγ*$^{-/-}$ animals, IL-17 neutralization and
321 celecoxib treatment led to different outcomes. For example, IL-17 neutralization or celecoxib
322 treatment alone reduced PMN infiltration but had no impact on CFU in PMNs and whole
323 lung, while celecoxib treatment, in addition to IL-17 neutralization, led to both - decline in
324 PMN infiltration and bacterial burden (Fig. 4). We re-analyzed our FACS data to explore
325 whether there are different subtypes of PMNs which differently associated with the bacterial
326 burden. We observed at least two distinct PMN sub-populations, grossly separated as low and
327 high FSC on the FSC-SSC plot (Fig. S5A). Interestingly, animals that received anti-IL-17
328 mAb and celecoxib together had a higher ratio of FSC^{high} to FSC^{low} PMNs than other groups
329 (Fig. S5B-D). Since this group showed the least PMN-resident *Mtb* and lower burden in the
330 lungs and spleen, FSC^{high} PMNs appear to be more restrictive towards *Mtb*, whereas FSC^{low}
331 PMNs appear more permissive or pathological. These sub-types need further characterization
332 to understand their true nature.

333 **Inhibiting RORγt breaks the PMN-IL-17 axis in WT animals and facilitates celecoxib-**
334 **mediated control of TB.**

335 IL-17 production by Th_{17} cells and PMNs is driven by the transcription factor RORγt (Berry
336 et al., 2010; Tan et al., 2013). While in *Mtb*-infected *IFNγ*$^{-/-}$ animals, IL-17 levels were very
337 high, even the WT animals showed an increase in IL-17 levels upon *Mtb* infection, albeit to a
338 lower magnitude than the *IFNγ*$^{-/-}$ mice (Fig. S5E, Fig. 3F). Since the WT mice, like *IFNγ*$^{-/-}$
339 mice, also showed substantial IL-17-Ly6G co-staining (Fig. 4C), we reasoned that a similar

340 IL-17-PMN axis could also be operating in the WT animals and contribute to sustained PMN-
341 resident pool of *Mtb* in the lungs. To test this hypothesis, we decided to inhibit RORγt in
342 *Mtb*-infected WT mice (Fig. 6A). Treatment with RORγt inhibitor SR2211 (inverse agonist)
343 led to a significant decline in IL-17 levels in the lung homogenates (Fig. 6B). Interestingly,
344 unlike the *Mtb*-infected *IFNγ*$^{-/-}$ mice, celecoxib alone also was able to reduce the level of IL-
345 17 in the lung homogenates of *Mtb*-infected WT mice, and so was the combination of both
346 SR2211 and celecoxib (Fig. 6B). To our surprise, SR2211 treatment also led to a loss of IL-
347 17-Ly6G co-staining, suggesting the role of PMN-derived IL-17 in disease pathology in the
348 WT mice (Fig. 6C). Treatment with SR2211 did not impact the PMN count in the lungs but
349 showed reduced PMN-resident *Mtb* population (Fig. 6D-E). Celecoxib, either alone or in
350 combination with SR2211, also reduced the intra-PMN *Mtb* load without impacting PMN
351 numbers (Fig. 6D-E). At the whole tissue level, SR2211 alone did not reduce *Mtb* burden in
352 the lungs. However, it was highly efficient in controlling dissemination to the spleen (Fig.
353 6F). Similarly, celecoxib treatment, either alone or in combination with SR2211, significantly
354 reduced bacterial CFUs in lung and spleen; however, the effects were more pronounced in the
355 spleen (Fig. 6F). The histopathology analysis of the lungs reflected the protective effects of
356 SR2211 and celecoxib (Fig. S6A-B). Treatment with SR2211 and celecoxib also impacted
357 the numbers of lung macrophages and MSCs and the resident bacterial population in
358 macrophages (Fig. S6C-F). Our data show that an IL-17-PMN axis gets established during
359 *Mtb* infection, which, if uncontrolled, could lead to severe pathology and disease. At the same
360 time, the results also provide a mechanistic basis for exploring RORγt inhibition as an adjunct
361 to preventive and therapeutic approaches against TB.

362 **RORγt inhibition enhances the protective efficacy of BCG in WT mice**

363 Since BCG vaccination failed to control the PMN-resident *Mtb* population, and our
364 subsequent results showed a strong influence of IL-17 on PMN recruitment and function, we

365 wondered whether blocking IL-17 could also enhance BCG efficacy, specifically by targeting
366 the PMN-resident *Mtb* population. So next, we treated BCG-vaccinated, *Mtb*-infected WT
367 mice with SR2211 (Fig. 6G). Treating BCG-vaccinated, *Mtb*-infected WT mice with SR2211
368 led to a ~3-fold reduction in the PMN-resident pool of *Mtb* (Fig. 6H). This also led to a more
369 than 7-fold decline in the total bacterial burden seen in the lungs of these mice (Fig. 6I).
370 Thus, together, these results indicate that the pro-pathogenic role of IL-17 also negatively
371 impacts the efficacy of BCG vaccination.

372 **The IL-17-Neutrophil axis in human TB subjects**

373 The results so far establish the role of the IL-17-PMN axis in TB pathology in mice. To
374 verify the existence of a similar axis in human TB, we took help from a prospective cohort
375 study of pulmonary tuberculosis (PTB). This study comprised 201 subjects of PTB, who were
376 treated for 6-8 months and followed up for an additional one year to track any recurrence
377 (Kumar et al., 2021; Kumar et al., 2020). Among those, 133 subjects were cured of PTB after
378 the full anti-TB treatment (ATT) regime (Fig. 7A). The cohort also had 68 subjects that failed
379 the standard ATT regime and showed manifestation of TB recurrence and death (Fig. 7A).
380 We compared this cohort's IL-17 and neutrophil levels at the time of recruitment (under
381 treatment-naïve conditions). The failed treatment group had significantly higher serum IL-17
382 levels at the time of recruitment (Fig. 7B). Moreover, the treatment failure group also had a
383 significantly higher absolute blood-neutrophil count and an increased neutrophil-to-
384 lymphocyte ratio (NLR) at the time of recruitment (Fig. 7C-D). Thus, the IL-17-PMN axis
385 appears to influence TB pathogenesis in both mice and humans, thereby providing an
386 opportunity to develop a protective strategy by targeting this axis.

387 **Discussions**

388 The immune response elicited by *Mtb* infection triggers the recruitment of diverse innate and
389 adaptive immune cells to the site of infection, leading to the formation of granulomas
390 (Ramakrishnan, 2012). A variety of infiltrating innate cells are expected to phagocytose and
391 kill the pathogen. However, *Mtb* coopts these cells and uses them as a niche to evade adaptive
392 immune response during the chronic phase (Chandra et al., 2022; Lee et al., 2020; Lovewell
393 et al., 2021). For example, different monocyte and macrophage populations in the lungs are
394 reported as major immune cells harbouring the intracellular *Mtb* in the lungs of infected mice,
395 which may also impact *Mtb* growth and survival differentially (Lee et al., 2020), (Huang et
396 al., 2018). Similarly, MSCs are shown to offer an immune-privileged niche to the *Mtb*,
397 protecting them from inflammatory cytokines (Jain et al., 2020). In *Mtb*-infected mice lungs,
398 neutrophils were reported to have the highest number of bacilli early during the
399 infection(Huang et al., 2018), while another study showed Ly6G^{+} granulocytes as a
400 permissive niche to *Mtb*(Lovewell et al., 2021; Mishra et al., 2017). In TB patients,
401 neutrophils are the most predominant infected phagocytes in the sputum samples, BAL fluid
402 and lung cavities (Eum et al., 2010). Extending the results from human patient studies and
403 mice experiments described above, counting CFUs from the cells sorted from infected mice's
404 lungs, we also observed that PMNs contained the largest pool of intracellular bacilli.
405 The role of neutrophils in impeding the protective response of BCG vaccination was
406 unexpected. While certain innate immune responses of BCG-vaccinated animals are
407 attributed to the trained immunity (Kaufmann et al., 2018), it is also reported that BCG
408 vaccination results in neutrophil reprogramming, leading to an enhanced anti-bacterial state
409 (Moorlag et al., 2020). We did observe depletion in the neutrophil-resident *Mtb* population,
410 suggesting an anti-bacterial activation state. However, they continued to represent the largest,
411 if not the only, pool of intracellular bacilli in those animals. Could the anti-bacterial state of

412 neutrophils in BCG-vaccinated animals be further enhanced? It is reported that BCG-
413 dependent COX-2/PGE2 pathway activation blunts macrophage, DC and PMN responses
414 (Ballinger et al., 2006; Serezani et al., 2007; Sheppe and Edelmann, 2021). This has led to
415 explorations on a combination of BCG with selective COX2 inhibitors to ameliorate the
416 efficacy of BCG (EP2763666B1) (Ibrahim et al., 2021). Curiously, selective COX-2
417 inhibition by celecoxib had no impact on neutrophil numbers in the lungs; it significantly
418 reduced the *Mtb* load in the neutrophils in BCG-vaccinated animals. Thus, our results show
419 that the COX2 pathway contributes to lower the efficacy of BCG-mediated protection by
420 preventing the anti-bacterial functions of neutrophils. The COX-2-mediated negative
421 regulation of neutrophil anti-bacterial response is also shown in the case of
422 *P. aeruginosa* infection (Sadikot et al., 2007).
423 Neutrophil infiltration to the site of infection depends on several factors. Chemotactic stimuli
424 like CXCL1, CXCL2, CCL2 and CCL7 can trigger neutrophil chemotaxis under resting or
425 activated states (Souto et al., 2011). Each of the four chemokines was upregulated to a
426 varying degree upon *Mtb* infection. In addition, IL-17 is also implicated in neutrophil
427 recruitment across different settings (Flannigan et al., 2017; Gelderblom et al., 2012). In TB,
428 IL-17 from $CD4^+$ T cells is believed to trigger neutrophil infiltration (Nandi and Behar,
429 2011). Interestingly, IFNγ can block IL-17 production and, therefore, serves as the
430 mechanism for high neutrophilia in *IFNγ*$^{-/-}$ mice upon *Mtb* infection (Nandi and Behar,
431 2011). We also observed very high lung neutrophil infiltration and lung IL-17 levels in *Mtb*-
432 infected *IFNγ*$^{-/-}$ mice. However, instead of Th_{17} cells, our results show that neutrophils are a
433 major source of IL-17 in *IFNγ*$^{-/-}$ mice. Since neutrophils also express IL-17 receptors, it
434 appears to establish an autocrine self-amplification loop contributing to severe disease
435 pathology. Surprisingly, COX2 inhibition, which helps control *Mtb* in the WT mice, fails to
436 do the same in *IFNγ*$^{-/-}$ mice unless the high IL-17 levels were also neutralized. The crosstalk

437 between prostaglandins and IL-17 is reported as they help Th_{17} cell differentiation
438 (Napolitani et al., 2009). However, our results show that IL-17, in addition to being produced
439 by Th_{17} cells, was also produced by neutrophils in *IFNγ*$^{-/-}$ mice and therefore, COX2
440 inhibition could have an independent mechanism through which it synergized with IL-17
441 neutralization to control *Mtb*. Neutrophils are known to express COX2 under inflammatory
442 conditions and secrete PGE2 (Maloney et al., 1998). Also, PGE2 can regulate neutrophil
443 migration, specifically when induced by IL-23/IL-17 (Lemos et al., 2009). However, we
444 suspect PGE2 also somehow curtail the antibacterial responses of neutrophils since we did
445 observe conditions where without a drop in neutrophil count, the intra-PMN bacillary load
446 reduced significantly upon COX2 inhibition.
447 Inhibiting RORγt with SR2211 provided further insights into the crosstalk between IL-17 and
448 COX2. RORγt is a classic nuclear receptor implicated with the Th_{17} cell differentiation
449 (Ivanov et al., 2006). Neutrophils express RORγt and IL-17 and can be activated through
450 autocrine IL-17A-IL-17RC interactions during fungal infections (Taylor et al., 2014).
451 However, the IL-17-mediated autocrine activation of neutrophils is believed to elicit strong
452 anti-microbial functions in the neutrophils (Taylor et al., 2014). While our data does indicate
453 a potential autocrine IL-17 signaling in the neutrophils of both *Mtb*-infected WT or *IFNγ*$^{-/-}$
454 mice, it does not appear to induce an antibacterial state but rather facilitates bacterial survival
455 and pathology. Inhibiting RORγt almost entirely wiped-out IL-17 levels in the lung
456 homogenates, and, to a large extent, it appeared to impact via inhibiting IL-17 production by
457 the neutrophils. Moreover, similar to the results obtained with IL-17 neutralization and COX2
458 inhibition in *IFNγ*$^{-/-}$ mice, inhibiting both RORγt and COX2 worked even in WT mice,
459 leading to significant control of bacterial load in the sorted cells as well as the whole lung and
460 spleen. Thus overall, IL-17-PMN crosstalk appears to restrain the protective host responses in
461 normal as well as highly susceptible models of TB. Finally, results with RORγt inhibition in

462 BCG-vaccinated animals suggest potential ways to enhance the efficacy of TB vaccines.
463 Whether a prophylactic regimen involving RORγt inhibition to high-risk individuals could
464 protect them from active disease is worth exploring. The results in this study also
465 inadvertently provided evidence for an anecdote, which is not usually proven experimentally
466 in TB disease. In all conditions where the neutrophil population or resident PMN were
467 targeted, either by celecoxib, IL-17 neutralization or SR2211 treatment, irrespective of the
468 impact on the bacillary load in the lungs, dissemination to the spleen was significantly
469 curtailed. This is in agreement with the reports that neutrophils play a direct role in the
470 dissemination of *Mtb* to other extrapulmonary sites (Hult et al., 2021).
471 Finally, the results on the human cohort re-emphasize the primacy of neutrophils in
472 determining the disease outcome in humans. We found that high neutrophils and IL-17 can
473 predict treatment failure. This underscores a similar neutrophil-IL-17 axis operational in
474 humans underlying disease severity, as reported in the mouse model in this study.
475 Interestingly, a neutrophil-driven transcriptional signature was earlier reported to be
476 associated with active TB (Berry et al., 2010). It is noteworthy that high neutrophilia alone
477 has been shown to predict death in TB patients (Lowe et al., 2013).
478 Finally, the results from mice lacking IFNγ have immediate clinical application. A relatively
479 small fraction, but a sizeable number of TB cases, belong to a category known as Mendelian
480 Susceptibility to Tubercular Diseases or MSMD, which typically is caused by a mutation in
481 the IFNγ/IL12p70 pathway, which also acts via regulating IFNγ (Filipe-Santos et al., 2006;
482 Kerner et al., 2020; Levin et al., 1995). These patients develop serious diseases even upon
483 exposure to BCG and respond poorly to anti-TB treatment (Casanova et al., 1995;
484 Mahdaviani et al., 2022). We believe the MSMD phenotype could be a manifestation of the
485 IL-17-PMN axis observed in *IFNγ*$^{-/-}$ animals. Thus, IL-17 neutralization or RORγt inhibition
486 could facilitate better treatment outcomes in these patients.

487 To conclude, through this study, we experimentally establish PMNs as a niche for *Mtb* under
488 normal and severe disease conditions, which is largely regulated by PMN-derived IL-17 as
489 well as the COX2 pathway. Targeted inhibition of IL-17 and COX2 can be exploited to
490 enhance the efficacy of BCG or other vaccine candidates and as adjunct therapeutic strategies
491 for the normal population and among those with genetic vulnerability towards severe TB.

492 **Materials and Methods:**

493 **Ethical clearance**

494 ITB biopsy samples and control samples were obtained from the Department of Pathology,
495 AIIMS, New Delhi. These biopsy samples were taken from the patients for diagnostic purposes
496 after taking their written informed consent. The use of the archived leftover biopsy samples
497 was approved by the institute's EC of AIIMS (Ref no. IEC-304/02-06-2017), and ICGEB (Ref
498 no. ICGEB/IEC/2017/06-verII and ICGEB/IEC/2016/03) and the same were accessed
499 according to the institutional guidelines. Animal experiments were approved by Institutional
500 Animal Ethics Committee, ICGEB (ICGEB/IAEC/280718/CI-14),
501 (ICGEB/IAEC/07032020/CI-18), and (ICGEB/IAEC/18092021/CI-16). The study on human
502 PTB subjects was approved by the Ethics Committees of the Prof. M. Viswanathan Diabetes
503 Research Center (ECR/51/INST/TN/ 2013/MVDRC/01) and NIRT (NIRT-INo:2014004).
504 Informed written consent was obtained from all participants. All the methods were performed
505 in accordance with the relevant institutional ethical committee guidelines.

506 **Reagents and antibodies**

507 Tween-20 (P1379), Vectashield (F6182), Triton-X-100 (9036-19-5), DNase 1 (D5025),
508 Collagenase D (11088858001), Propidium Iodide (P4170), HBSS (H6648), Trizol (T9424),
509 Hematoxylin (51275), Eosin (318906), Formalin (HT501128), Celecoxib (SML3031-50MG),
510 DAPI (28718-90-3), Xylene (CAS-1330-20-7), Absolute ethanol (CAS- 64-17-5), Sodium
511 Citrate (CAS--6132-04-3) were obtained from Sigma-Aldrich. SR 2211, Selective RORγt
512 inverse agonist (4869) was procured from TOCRIS. 7H9 (271310), 7H11 (212203), ADC
513 (211887), OADC (211886) FACS Flow Sheath Fluid (342003), Accudrop Fluorescent Beads
514 (345249), CS&T Research Beads Kit (655050), all FACS antibodies used for acquisition and
515 sorting (details are provided in the separate table) were procured from Becton Dickinson

516 Private Limited. Fixable Viability Dye eFluor™ 780 used for live/dead staining was obtained
517 from eBioscience™. InVivoMAb anti-mouse IL-17A (BE0173), InVivoPure pH 7.0 Dilution
518 Buffer (IP0070), InVivoMAb mouse IgG1 isotype control, unknown specificity (BE0083),
519 InVivoPure pH 6.5 Dilution Buffer (IP0065) were purchased from BioXcell. Mouse IL-17A
520 ELISA Kit (ab199081), mouse PGE2 ELISA Kit (ab287802and Cytokine & Chemokine 36-
521 Plex Mouse ProcartaPlexTM Panel 1A (EPX360-26092-901) for Luminex assay were obtained
522 from Abcam and Thermofisher respectively. Penta antibiotic mix (FD260-5VL) was procured
523 from Himedia.

524 **Mycobacterial cultures**

525 Bacterial strains: Lab-adapted strain of *Mycobacterium tuberculosis*, H37Rv, seed stock was
526 received from Colorado State University. BCG (Pasteur strain) was obtained from the National
527 Institute of Immunology, New Delhi. For *Mtb* ex-vivo and in-vivo infection experiments,
528 H37Rv and BCG mycobacterial cultures were grown in 7H9 media (BD Difco) supplemented
529 with 10% Albumin–Dextrose–Catalase (ADC, BD, Difco) and incubated in an orbiter shaker
530 at 100 rpm, 37 °C till the growth reach to the log phase. The log phase cultures were pelleted
531 down, and the pellet was resuspended in either saline (for aerosol infection in mice) or culture
532 media (for ex-vivo infection in cells). Single-cell suspensions of H37Rv and BCG were
533 prepared by passing bacterial cultures seven times through 23-gauge needles, five times
534 through 26-gauge needles, and three times through 30-gauge needles.

535 **Animals**

536 WT C57BL/6 mice were procured from animal house, ICGEB, New Delhi and *IFNγ*$^{-/-}$ C57BL/6
537 mice were procured from animal house, NII, New Delhi. Both male and female, six to eight
538 weeks old mice were used for all the in vivo experiments. *Mtb*-infected mice were housed in
539 our biosafety level-3 laboratory and kept pathogen-free by routine serological and

540 histopathological examinations. Animal protocols employed in this study were approved by
541 the Institutional Animal Ethics Committee.

542 **Aerosol challenge in C57BL/6 mice with H37Rv strain**

543 All mice experiments were carried out in the Tuberculosis Aerosol Challenge Facility (TACF,
544 ICGEB, New Delhi, India). C57BL/6 mice were housed in cages within a biosafety level 3
545 laminar flow enclosure. According to the standardized protocol, mice were infected with 100-
546 200 CFU (unless otherwise stated) with H37Rv in a Wisconsin-Madison chamber. To confirm
547 the infection establishment and to enumerate the exact CFU delivered, two animals were
548 selected randomly and humanely euthanized 24 hours post-aerosol challenge. The lung tissues
549 were harvested and homogenized in 1X PBS, followed by plating on Petri plates containing
550 Middlebrook 7H11 agar (Difco) supplemented with 10% OADC (Becton, Dickinson) 0.5%
551 glycerol. The colonies were counted after 21 days to enumerate the *Mtb* load.

552 **Drug treatment and BCG vaccination of mice**

553 Cox-2 inhibitor Celecoxib (50mg/kg) was administered to the mice through oral gavaging once
554 per day, according to the timeline of the experiment. RORγt inhibitor SR2211 (20mg/kg) was
555 administered to the mice through intra-peritoneal route every alternate day according to the
556 timeline of the experiment. Mice were vaccinated with BCG intradermally at a dose of 1 million
557 bacilli per mouse.

558

559 **CFU plating post *Mtb*-Infection**

560 At various time-points post *Mtb*-infection, lung, and spleen tissues were harvested from the
561 infected mice. The left half lung of the mice was homogenized and serial diluted in 1X PBS.
562 Different dilutions were plated in duplicates on 7H11 agar plates supplemented with 10%
563 OADC to get *Mtb* colonies within the countable range. Similarly, spleens were also harvested,

564 homogenized, and serially diluted in 1X PBS, followed by plating on 7H11 agar plates. The
565 colonies were counted after 21 days to enumerate the *Mtb* load.

566 **FACS sample preparation**

567 The right half lung of the infected mice was used in the preparation of single cell suspension
568 followed by FACS sorting and subsequent plating of sorted cells (i.e., Neutrophils,
569 Macrophages, and Mesenchymal stem cells. For sorting, the tissue was washed with 1X PBS
570 and chopped into small pieces. 20U/ml DNase 1 and 1mg/ml collagenase D were added to the
571 chopped tissue and incubated for 30-45 minutes at 37ºC. After incubation, the chopped lung
572 tissues were passed through the nylon mesh of a 70-micron cell strainer to get a single-cell
573 suspension. The cells were pelleted at 1200 rpm, and the cell pellet was treated with 1X ACK
574 RBC lysis buffer to get rid of RBCs and washed with 1X PBS. The cells were incubated with
575 Fc-Block antibody (CD16/32 FCR-γ antibody) on ice for 15 minutes to inhibit the binding of
576 surface antibodies to Fc receptors on the immune cell surface. The cells were washed with PBS
577 and subsequentially stained with the antibody cocktail of CD45.2, CD11b, Ly6G, MHCII,
578 CD64, MerTK, Sca-1, CD90.1, and CD73 and placed on ice for 45 minutes. Dead cells were
579 stained with fixable viability dye eFluor™ 780 (FVD eFluor 780) or Propidium Iodide (PI)at
580 five µg/ml concentration just before acquisition.

581 **FACS cell sorting**

582 After staining and washing, the lung cells were again passed through a 40-micron strainer
583 before acquisition into the FACS machine to ensure formation of single-cell suspension. The
584 whole sample was acquired to get the maximum number of live sorted cells (Neutrophils,
585 Macrophages, and Mesenchymal stem cells). The sorted cells were then pelleted (at 13000
586 RPM), lysed, and plated on 7H11 plates. The colonies were counted after 21 days to enumerate
587 the *Mtb* burden within each sorted cell type.

588 **RNA-Seq analysis**

589 Reads were quality filtered using Trimmomatic (v.0.39, LEADING:10 TRAILING:10
590 SLIDING WINDOW:4:15 MINLEN:75) (Bolger et al., 2014) and were assessed for quality
591 using FastQC (v.10.1) (Andrews, 2010) and visualised with MultiQC (v.1.9) (Ewels et al.,
592 2016). Salmon (v.1.8, –numGibbsSamples 30) (Patro et al., 2017) was used to quantify quality
593 filtered reads against mouse genome (GRCm39, primary assembly) with Gencode annotation
594 (v.M30) (Frankish et al., 2019). Profiles were imported using tximeta (v.1.10) (Love et al.,
595 2020) and SummarizedExperiment (v.1.22) (Morgan et al., 2018) which were then summarised
596 to gene-level expression. Following biotypes were filtered out: pseudogenes, TEC, snRNA,
597 lncRNA, miRNA, snoRNA, misc_RNA, rRNA, ribozyme, scaRNA, sRNA, scRNA,
598 Mt_tRNA, Mt_rRNA. Dataset was further filtered to remove features not expressed across the
599 whole dataset. The dataset was normalised to scaled TPM values. Downstream analyses are
600 described in the statistical analyses section.

601 **Multiplex Microbead-based Immunoassay (Luminex)**

602 Mouse lung homogenates were collected for Luminex analysis using the Cytokine &
603 Chemokine 36-Plex Mouse ProcartaPlexTM Panel 1A (ThermoFisher, # EPX360-26092-
604 901). Samples were incubated with fluorescent-coded magnetic beads pre-coated with
605 respective antibodies in a black 96-well clear-bottom plate overnight at 4 °C. After
606 incubation, plates were washed 5 times with wash buffer (PBS with 1% BSA (Capricorn
607 Scientific) and 0.05% Tween-20 (Promega)). Sample- antibody-bead complexes were
608 incubated with Biotinylated detection antibodies for 1h and washed 5 times. Subsequently,
609 Streptavidin-PE was added and incubated for another 30 mins. Plates were washed 5 times,
610 before sample-antibody-bead complexes were re-suspended in sheath fluid for acquisition on
611 the FLEXMAP® 3D (Luminex) using xPONENT® 4.0 (Luminex) software. Data analysis
612 was done using Bio-Plex ManagerTM 6.1.1 (Bio-Rad). Standard curves were generated with

613 a 5-PL (5-parameter logistic) algorithm, reporting values for both mean florescence intensity
614 (MFI) and concentration data.

615 **Tissue Immunofluorescence Assay (IFA)**

616 Five-micron thick sections of paraffin-embedded tissue sections were taken in poly-L-Lysine
617 coated slide. Deparaffinization was performed by heating the slides at 50 °C for 20 seconds
618 till the wax melts, followed by the subsequent steps, 100% xylene for 10 minutes, xylene and
619 absolute ethanol for 10 minutes, 100% ethanol for 10 minutes, 70% percent ethanol for 5
620 minutes, 50% ethanol, distilled water for 5 minutes and a final wash in 1x PBS for 5 minutes.
621 Antigen retrieval was performed in antigen retrieval buffer (10mM Sodium Citrate, 0.05%
622 tween-20, pH: 6) by heating the slides at 100 ºC for 15 minutes. After antigen retrieval,
623 permeabilization was performed with 0.04% Triton-X 100 in 1X PBS (0.04% PBST) for 20
624 minutes followed by proper washing with 1X PBS. Blocking was done by 3% BSA for 1
625 hour. Sequential addition of primary antibody was performed at 1:100 dilution at 4 ºC
626 overnight. Primary antibody was washed with 1X PBS followed by counter stain with DAPI
627 nuclear stain at 1 ug/ml concentration. Mounting was done with a drop of vectashield.

628 **Histopathological studies**

629 Formalin fixed tissue samples (<5mm thick) were washed under running water for 4-12
630 hours. Tissue dehydration was performed in ascending grades of alcohol (30%, 50%, 70%,
631 90%, 95%) followed by two washes in absolute alcohol, one hour each and two washes in
632 xylene for one hour each. Paraffinization in melted paraffin wax (57-60 ºC) was performed
633 three times sequentially for one hour each. FFPE (formalin fixed paraffin embedded) tissue
634 blocks were prepared by placing tissue and melted paraffin in steel moulds. Five micrometres
635 thick sections of tissue were cut with the help of microtome. Tissue sections were allowed to
636 float on water bath (45-50 ºC) and placed on clean glass slide. Deparaffinization was
637 performed by three sequential washes in xylene for 5 minutes each followed by hydration in

638 descending grades of alcohol (absolute alcohol, 90% and 70%) followed by one wash in
639 water, 5 minutes each. For H&E staining, slides were first stained with haematoxylin (it
640 stains the nucleus blue) for 5-10 minutes followed by one wash with water. The slides were
641 subsequently stained with Eosin (it stains the cytoplasm pink) for 5-10 minutes followed by
642 one wash with absolute alcohol and one wash with xylene. Slides were mounted with
643 coverslips followed by sealing with DPX. Images were acquired on Zeiss microscope.

644 **<u>In vivo IL-17 Neutralization experiment</u>**

645 IFNγ knock out C57BL/6 mice were challenged with 100-200 CFU with H37Rv via the aerosol
646 route (as described previously). The anti-mouse IL-17 monoclonal Ab was administered via
647 intra-peritoneal route at a dose of 100 milligrams per mouse every 3–4 days starting one day
648 before *M. tuberculosis* infection for the duration of the study, i.e., six weeks. Control groups
649 received matched IgG isotypes. Six weeks post *Mtb* infection, mice were treated with 50mg/kg
650 celecoxib through oral route for the duration of the experiments. Mice in all experimental
651 groups were sacrificed at 6 weeks post infection, according to the experimental timeline. The
652 left half lungs and whole spleen of the mice were homogenized and serially diluted in 1X PBS.
653 Different dilutions were plated in duplicates on 7H11 agar plates and the colonies were counted
654 after 21 days to enumerate the *Mtb* load. The middle lobe of the right lung was preserved in
655 formalin for Histopathology and IFA studies. The rest part of the right half lung of the infected
656 mice was used in the preparation of single cell suspension. The single cell suspension was
657 divided into two parts and stained with different antibody cocktails. One part was used for
658 FACS sorting and subsequent plating of sorted cells (i.e., Neutrophils, Macrophages, and
659 Mesenchymal stem cells) and the other half was used for FACS acquisition to enumerate Th17
660 cells inside the lungs. Sera was also collected to quantify IL17 levels.

661 **IL-17/PGE2 ELISA**

662 IL-17 levels and PGE2 levels in the lung homogenates of uninfected mice, *Mtb*-infected mice,
663 *Mtb*-infected treated mice from various experimental groups were measured using ELISA kits
664 procured from Abcam using the manufacturer's protocol.
665
666 **Study Population (PTB subjects)**
667 Participants were enrolled from the Effect of Diabetes on Tuberculosis Severity (EDOTS)
668 study, a prospective cohort study conducted in Chennai, India. A total of 68 had unfavourable
669 treatment outcomes, comprising treatment failure, relapse, or death. Inclusion criterion was
670 new smear and culture-positive adults (age 18-75 years). Exclusion criteria were previous
671 treatment for TB, drug resistant TB, HIV positivity or taking immunosuppressive drugs, and
672 >7 days of anti-TB treatment prior to enrolment. As part of our study protocol HIV screening
673 was done for all the study participants. The diagnosis of PTB was established by positive
674 sputum culture on solid media with compatible chest X-ray. Anti-TB treatment (ATT) was
675 provided by government TB clinics according the Revised National Tuberculosis Control
676 Programme standards in effect at that time. Participants were followed up monthly through the
677 six months course of treatment and every three months thereafter till one year after treatment
678 completion Cure was defined as negative sputum cultures at months 5 and 6 of treatment.
679 Adverse treatment outcomes included treatment failure defined as positive sputum culture at
680 months 5 or 6, all-cause mortality over the duration of treatment, or recurrent TB demonstrated
681 by positive sputum smear and culture with compatible symptoms or chest X-ray within twelve
682 months after initial cure. There was a total of 18 TB treatment failures, 16 deaths and 34 TB
683 recurrences. Case-control matching was based on age, gender, body mass index (BMI), and
684 diabetic status. Peripheral blood was collected in heparinized tubes. Following centrifugation,
685 plasma was collected and stored at -80 ^{o}C till further analysis. Baseline sample collection was

686 performed at enrolment. The demographic and epidemiological data for this cohort have been
687 previously reported (Kumar et al., 2021; Kumar et al., 2020).

688 **Multiplex assays**

689 Circulating plasma levels of cytokines and chemokines were measured using the Luminex
690 MAGPIX Multiplex Assay system (Bio-Rad, Hercules, CA). Luminex Human Magnetic Assay
691 Kit 45 Plex (R&D Systems) was used to measure the cytokines and chemokine levels

692 **Statistical analysis**

693 Transcriptomics analyses were done in R statistical software environment (v.4.1) (Team,
694 2021). Statistical analysis was done using swish methodology from fishpond (v.1.8) (Zhu et
695 al., 2019) and significantly differentially expressed genes (DEGs) were defined based on
696 *qvalue* ≤ 0.1 and absolute $\log_2$ fold change ≥ 1. Heatmap of the DEGs was generated with
697 ComplexHeatmap (v.2.8) using mean z-scaled values and clustered based on Euclidean
698 distance and Ward.D2 methodology. Enrichment analysis was done using clusterProfiler (v.
699 4.0.5) (Wu et al., 2021) and simplify function was used to reduce the GO BP terms at a
700 similarity cutoff of 0.5 as applicable. Significance of enrichment defined by nominal p-value
701 ≤ 0.05 unless stated otherwise. Other figures from RNASeq analyses were generated using
702 ggplot2 (v.3.3.5) (Wickham, 2016).

703

704 **Data availability**

705 The raw RNAseq data used for this study is available at the GEO database with the accession
706 number: **GSE238265.**

707 **Funding:** The work on this project was supported by Department of Biotechnology (BT/IC-
708 06/003/91-Flagship program to DK), MDR-TB project from Department of Biotechnology
709 (BT/PR23092/NER/95/589/2017, DK) and SR-National Bioscience Award from Department
710 of Biotechnology (BT/HRD/NBA-NWB/39/2020-21 (4), DK). The research in DK lab is also

711 supported by DBT-Wellcome Trust India Alliance Senior Fellowship (IA/S/17/1/503071) and
712 extramural research grants from SERB (EMR/2016/005296 to DK). Priya Sharma is a
713 recipient of a fellowship from the Indian Council of Medical Research (3/1/3/JRF-
714 2017/HRD-LS/55193/79). Raman Deep Sharma is a recipient of a fellowship from
715 Department of Biotechnology (DBT/JRF/BET-18/I/2018/AL/160).
716

717 **Acknowledgements**

718 We thank the Tuberculosis Aerosol Challenge Facility (TACF), supported by the Department
719 of Biotechnology, Govt of India, for supporting the BSL3 facility. We thank the staff of the
720 Department of Clinical Research and the Department of Bacteriology, NIRT for valuable
721 assistance in bacterial cultures and radiology and the staff of Prof. M. Viswanathan Diabetes
722 Research Center, RNTCP and Chennai corporation for valuable assistance in recruiting the
723 patients for this study. Data in this manuscript were collected as part of the Regional
724 Prospective Observational Research for Tuberculosis (RePORT) India Consortium.

725
726 **References:**
727
728 Allen, J.E., T.E. Sutherland, and D. Ruckerl. 2015. IL-17 and neutrophils: unexpected players
729 in the type 2 immune response. *Curr Opin Immunol* 34:99-106.
730 Andrews, S. 2010. FastQC: A Quality Control Tool for High Throughput Sequence Data. In.
731 Ballinger, M.N., D.M. Aronoff, T.R. McMillan, K.R. Cooke, K. Olkiewicz, G.B. Toews, M.
732 Peters-Golden, and B.B. Moore. 2006. Critical role of prostaglandin E2
733 overproduction in impaired pulmonary host response following bone marrow
734 transplantation. *J Immunol* 177:5499-5508.
735 Barry, C.E., 3rd, H.I. Boshoff, V. Dartois, T. Dick, S. Ehrt, J. Flynn, D. Schnappinger, R.J.
736 Wilkinson, and D. Young. 2009. The spectrum of latent tuberculosis: rethinking the
737 biology and intervention strategies. *Nat Rev Microbiol* 7:845-855.
738 Basile, J.I., L.J. Geffner, M.M. Romero, L. Balboa, Y.G.C. Sabio, V. Ritacco, A. Garcia, M.
739 Cuffre, E. Abbate, B. Lopez, L. Barrera, M. Ambroggi, M. Aleman, M.C. Sasiain, and
740 S.S. de la Barrera. 2011. Outbreaks of mycobacterium tuberculosis MDR strains
741 induce high IL-17 T-cell response in patients with MDR tuberculosis that is closely
742 associated with high antigen load. *J Infect Dis* 204:1054-1064.
743 Berry, M.P., C.M. Graham, F.W. McNab, Z. Xu, S.A. Bloch, T. Oni, K.A. Wilkinson, R.
744 Banchereau, J. Skinner, R.J. Wilkinson, C. Quinn, D. Blankenship, R. Dhawan, J.J. Cush,
745 A. Mejias, O. Ramilo, O.M. Kon, V. Pascual, J. Banchereau, D. Chaussabel, and A.
746 O'Garra. 2010. An interferon-inducible neutrophil-driven blood transcriptional
747 signature in human tuberculosis. *Nature* 466:973-977.
748 Bolger, A.M., M. Lohse, and B. Usadel. 2014. Trimmomatic: a flexible trimmer for Illumina
749 sequence data. *Bioinformatics* 30:2114-2120.
750 Brazier, B., and H. McShane. 2020. Towards new TB vaccines. *Semin Immunopathol* 42:315-
751 331.
752 Cadena, A.M., S.M. Fortune, and J.L. Flynn. 2017. Heterogeneity in tuberculosis. *Nat Rev*
753 *Immunol* 17:691-702.
754 Casanova, J.L., E. Jouanguy, S. Lamhamedi, S. Blanche, and A. Fischer. 1995. Immunological
755 conditions of children with BCG disseminated infection. *Lancet* 346:581.
756 Chandra, P., S.J. Grigsby, and J.A. Philips. 2022. Immune evasion and provocation by
757 Mycobacterium tuberculosis. *Nat Rev Microbiol* 20:750-766.
758 Chaves Torres, N.M., J.J. Quijano Rodriguez, P.S. Porras Andrade, M.B. Arriaga, and E.M.
759 Netto. 2019. Factors predictive of the success of tuberculosis treatment: A
760 systematic review with meta-analysis. *PLoS One* 14:e0226507.
761 Cooper, A.M., D.K. Dalton, T.A. Stewart, J.P. Griffin, D.G. Russell, and I.M. Orme. 1993.
762 Disseminated tuberculosis in interferon gamma gene-disrupted mice. *The Journal of*
763 *experimental medicine* 178:2243-2247.
764 Cruz, A., A.G. Fraga, J.J. Fountain, J. Rangel-Moreno, E. Torrado, M. Saraiva, D.R. Pereira, T.D.
765 Randall, J. Pedrosa, A.M. Cooper, and A.G. Castro. 2010. Pathological role of
766 interleukin 17 in mice subjected to repeated BCG vaccination after infection with
767 Mycobacterium tuberculosis. *The Journal of experimental medicine* 207:1609-1616.
768 Dallenga, T., and U.E. Schaible. 2016. Neutrophils in tuberculosis--first line of defence or
769 booster of disease and targets for host-directed therapy? *Pathog Dis* 74:
770 Dartois, V.A., and E.J. Rubin. 2022. Anti-tuberculosis treatment strategies and drug
771 development: challenges and priorities. *Nat Rev Microbiol* 20:685-701.

772 Das, B., S.S. Kashino, I. Pulu, D. Kalita, V. Swami, H. Yeger, D.W. Felsher, and A. Campos-
773 Neto. 2013. CD271(+) bone marrow mesenchymal stem cells may provide a niche for
774 dormant Mycobacterium tuberculosis. *Sci Transl Med* 5:170ra113.
775 Domingo-Gonzalez, R., S. Das, K.L. Griffiths, M. Ahmed, M. Bambouskova, R. Gopal, S. Gondi,
776 M. Munoz-Torrico, M.A. Salazar-Lezama, A. Cruz-Lagunas, L. Jimenez-Alvarez, G.
777 Ramirez-Martinez, R. Espinosa-Soto, T. Sultana, J. Lyons-Weiler, T.A. Reinhart, J.
778 Arcos, M. de la Luz Garcia-Hernandez, M.A. Mastrangelo, N. Al-Hammadi, R.
779 Townsend, J.M. Balada-Llasat, J.B. Torrelles, G. Kaplan, W. Horne, J.K. Kolls, M.N.
780 Artyomov, J. Rangel-Moreno, J. Zuniga, and S.A. Khader. 2017. Interleukin-17 limits
781 hypoxia-inducible factor 1alpha and development of hypoxic granulomas during
782 tuberculosis. *JCI Insight* 2:
783 Eum, S.Y., J.H. Kong, M.S. Hong, Y.J. Lee, J.H. Kim, S.H. Hwang, S.N. Cho, L.E. Via, and C.E.
784 Barry, 3rd. 2010. Neutrophils are the predominant infected phagocytic cells in the
785 airways of patients with active pulmonary TB. *Chest* 137:122-128.
786 Ewels, P., M. Magnusson, S. Lundin, and M. Kaller. 2016. MultiQC: summarize analysis
787 results for multiple tools and samples in a single report. *Bioinformatics* 32:3047-
788 3048.
789 Fatima, S., S.S. Kamble, V.P. Dwivedi, D. Bhattacharya, S. Kumar, A. Ranganathan, L. Van
790 Kaer, S. Mohanty, and G. Das. 2020. Mycobacterium tuberculosis programs
791 mesenchymal stem cells to establish dormancy and persistence. *J Clin Invest*
792 130:655-661.
793 Filipe-Santos, O., J. Bustamante, A. Chapgier, G. Vogt, L. de Beaucoudrey, J. Feinberg, E.
794 Jouanguy, S. Boisson-Dupuis, C. Fieschi, C. Picard, and J.L. Casanova. 2006. Inborn
795 errors of IL-12/23- and IFN-gamma-mediated immunity: molecular, cellular, and
796 clinical features. *Semin Immunol* 18:347-361.
797 Flannigan, K.L., V.L. Ngo, D. Geem, A. Harusato, S.A. Hirota, C.A. Parkos, N.W. Lukacs, A.
798 Nusrat, V. Gaboriau-Routhiau, N. Cerf-Bensussan, A.T. Gewirtz, and T.L. Denning.
799 2017. IL-17A-mediated neutrophil recruitment limits expansion of segmented
800 filamentous bacteria. *Mucosal Immunol* 10:673-684.
801 Flynn, J.L., J. Chan, K.J. Triebold, D.K. Dalton, T.A. Stewart, and B.R. Bloom. 1993. An
802 essential role for interferon gamma in resistance to Mycobacterium tuberculosis
803 infection. *The Journal of experimental medicine* 178:2249-2254.
804 Frankish, A., M. Diekhans, A.M. Ferreira, R. Johnson, I. Jungreis, J. Loveland, J.M. Mudge, C.
805 Sisu, J. Wright, J. Armstrong, I. Barnes, A. Berry, A. Bignell, S. Carbonell Sala, J. Chrast,
806 F. Cunningham, T. Di Domenico, S. Donaldson, I.T. Fiddes, C. Garcia Giron, J.M.
807 Gonzalez, T. Grego, M. Hardy, T. Hourlier, T. Hunt, O.G. Izuogu, J. Lagarde, F.J.
808 Martin, L. Martinez, S. Mohanan, P. Muir, F.C.P. Navarro, A. Parker, B. Pei, F. Pozo,
809 M. Ruffier, B.M. Schmitt, E. Stapleton, M.M. Suner, I. Sycheva, B. Uszczynska-
810 Ratajczak, J. Xu, A. Yates, D. Zerbino, Y. Zhang, B. Aken, J.S. Choudhary, M. Gerstein,
811 R. Guigo, T.J.P. Hubbard, M. Kellis, B. Paten, A. Reymond, M.L. Tress, and P. Flicek.
812 2019. GENCODE reference annotation for the human and mouse genomes. *Nucleic*
813 *Acids Res* 47:D766-D773.
814 Funk, C.D. 2001. Prostaglandins and leukotrienes: advances in eicosanoid biology. *Science*
815 294:1871-1875.
816 Gelderblom, M., A. Weymar, C. Bernreuther, J. Velden, P. Arunachalam, K. Steinbach, E.
817 Orthey, T.V. Arumugam, F. Leypoldt, O. Simova, V. Thom, M.A. Friese, I. Prinz, C.
818 Holscher, M. Glatzel, T. Korn, C. Gerloff, E. Tolosa, and T. Magnus. 2012.

819 Neutralization of the IL-17 axis diminishes neutrophil invasion and protects from
820 ischemic stroke. *Blood* 120:3793-3802.
821 Han, Y., S.J. Kim, S.H. Lee, Y.S. Sim, Y.J. Ryu, J.H. Chang, S.S. Shim, Y. Kim, and J.H. Lee. 2018.
822 High blood neutrophil-lymphocyte ratio associated with poor outcomes in miliary
823 tuberculosis. *J Thorac Dis* 10:339-346.
824 Heyckendorf, J., S. Marwitz, M. Reimann, K. Avsar, A.R. DiNardo, G. Gunther, M. Hoelscher,
825 E. Ibraim, B. Kalsdorf, S.H.E. Kaufmann, I. Kontsevaya, F. van Leth, A.M. Mandalakas,
826 F.P. Maurer, M. Muller, D. Nitschkowski, I.D. Olaru, C. Popa, A. Rachow, T. Rolling, J.
827 Rybniker, H.J.F. Salzer, P. Sanchez-Carballo, M. Schuhmann, D. Schaub, V. Spinu, I.
828 Suarez, E. Terhalle, M. Unnewehr, J. Weiner, 3rd, T. Goldmann, and C. Lange. 2021.
829 Prediction of anti-tuberculosis treatment duration based on a 22-gene
830 transcriptomic model. *Eur Respir J* 58:
831 Huang, L., E.V. Nazarova, S. Tan, Y. Liu, and D.G. Russell. 2018. Growth of Mycobacterium
832 tuberculosis in vivo segregates with host macrophage metabolism and ontogeny. *The*
833 *Journal of experimental medicine* 215:1135-1152.
834 Hult, C., J.T. Mattila, H.P. Gideon, J.J. Linderman, and D.E. Kirschner. 2021. Neutrophil
835 Dynamics Affect Mycobacterium tuberculosis Granuloma Outcomes and
836 Dissemination. *Front Immunol* 12:712457.
837 Ibrahim, O.M., P.H. Basse, W. Jiang, K. Guru, G. Chatta, and P. Kalinski. 2021. NFkappaB-
838 Activated COX2/PGE(2)/EP4 Axis Controls the Magnitude and Selectivity of BCG-
839 Induced Inflammation in Human Bladder Cancer Tissues. *Cancers (Basel)* 13:
840 Ivanov, II, B.S. McKenzie, L. Zhou, C.E. Tadokoro, A. Lepelley, J.J. Lafaille, D.J. Cua, and D.R.
841 Littman. 2006. The orphan nuclear receptor RORgammat directs the differentiation
842 program of proinflammatory IL-17+ T helper cells. *Cell* 126:1121-1133.
843 Jain, N., H. Kalam, L. Singh, V. Sharma, S. Kedia, P. Das, V. Ahuja, and D. Kumar. 2020.
844 Mesenchymal stem cells offer a drug-tolerant and immune-privileged niche to
845 Mycobacterium tuberculosis. *Nat Commun* 11:3062.
846 Jung, B.G., B. Samten, K. Dean, R.J. Wallace, Jr., B.A. Brown-Elliott, T. Tucker, S. Idell, J.V.
847 Philley, and R. Vankayalapati. 2022. Early IL-17A production helps establish
848 Mycobacterium intracellulare infection in mice. *PLoS Pathog* 18:e1010454.
849 Jurado, J.O., V. Pasquinelli, I.B. Alvarez, D. Pena, A.I. Rovetta, N.L. Tateosian, H.E. Romeo,
850 R.M. Musella, D. Palmero, H.E. Chuluyan, and V.E. Garcia. 2012. IL-17 and IFN-
851 gamma expression in lymphocytes from patients with active tuberculosis correlates
852 with the severity of the disease. *J Leukoc Biol* 91:991-1002.
853 Kaufmann, E., J. Sanz, J.L. Dunn, N. Khan, L.E. Mendonca, A. Pacis, F. Tzelepis, E. Pernet, A.
854 Dumaine, J.C. Grenier, F. Mailhot-Leonard, E. Ahmed, J. Belle, R. Besla, B. Mazer, I.L.
855 King, A. Nijnik, C.S. Robbins, L.B. Barreiro, and M. Divangahi. 2018. BCG Educates
856 Hematopoietic Stem Cells to Generate Protective Innate Immunity against
857 Tuberculosis. *Cell* 172:176-190 e119.
858 Kerner, G., J. Rosain, A. Guerin, A. Al-Khabaz, C. Oleaga-Quintas, F. Rapaport, M.J. Massaad,
859 J.Y. Ding, T. Khan, F.A. Ali, M. Rahman, C. Deswarte, R. Martinez-Barricarte, R.S.
860 Geha, V. Jeanne-Julien, D. Garcia, C.Y. Chi, R. Yang, M. Roynard, B. Fleckenstein, F.
861 Rozenberg, S. Boisson-Dupuis, C.L. Ku, Y. Seeleuthner, V. Beziat, N. Marr, L. Abel, W.
862 Al-Herz, J.L. Casanova, and J. Bustamante. 2020. Inherited human IFN-gamma
863 deficiency underlies mycobacterial disease. *J Clin Invest* 130:3158-3171.

Ketelut-Carneiro, N., C.O.S. Souza, L. Benevides, L.G. Gardinassi, M.C. Silva, L.A. Tavares, D.S. Zamboni, and J.S. Silva. 2019. Caspase-11-dependent IL-1alpha release boosts Th17 immunity against Paracoccidioides brasiliensis. *PLoS Pathog* 15:e1007990.

Kimmey, J.M., J.P. Huynh, L.A. Weiss, S. Park, A. Kambal, J. Debnath, H.W. Virgin, and C.L. Stallings. 2015. Unique role for ATG5 in neutrophil-mediated immunopathology during M. tuberculosis infection. *Nature* 528:565-569.

Kolaczkowska, E., and P. Kubes. 2013. Neutrophil recruitment and function in health and inflammation. *Nat Rev Immunol* 13:159-175.

Kumar, N.P., K. Moideen, A. Nancy, V. Viswanathan, K. Thiruvengadam, D. Nair, V.V. Banurekha, S. Sivakumar, S. Hissar, H. Kornfeld, and S. Babu. 2021. Plasma Chemokines Are Baseline Predictors of Unfavorable Treatment Outcomes in Pulmonary Tuberculosis. *Clin Infect Dis* 73:e3419-e3427.

Kumar, N.P., K. Moideen, A. Nancy, V. Viswanathan, K. Thiruvengadam, S. Sivakumar, S. Hissar, D. Nair, V.V. Banurekha, H. Kornfeld, and S. Babu. 2020. Association of Plasma Matrix Metalloproteinase and Tissue Inhibitors of Matrix Metalloproteinase Levels With Adverse Treatment Outcomes Among Patients With Pulmonary Tuberculosis. *JAMA Netw Open* 3:e2027754.

Lee, J., S. Boyce, J. Powers, C. Baer, C.M. Sassetti, and S.M. Behar. 2020. CD11cHi monocyte-derived macrophages are a major cellular compartment infected by Mycobacterium tuberculosis. *PLoS Pathog* 16:e1008621.

Lee, W.W., S.W. Kang, J. Choi, S.H. Lee, K. Shah, E.E. Eynon, R.A. Flavell, and I. Kang. 2010. Regulating human Th17 cells via differential expression of IL-1 receptor. *Blood* 115:530-540.

Leliefeld, P.H.C., J. Pillay, N. Vrisekoop, M. Heeres, T. Tak, M. Kox, S.H.M. Rooijakkers, T.W. Kuijpers, P. Pickkers, L.P.H. Leenen, and L. Koenderman. 2018. Differential antibacterial control by neutrophil subsets. *Blood Adv* 2:1344-1355.

Lemos, H.P., R. Grespan, S.M. Vieira, T.M. Cunha, W.A. Verri, Jr., K.S. Fernandes, F.O. Souto, I.B. McInnes, S.H. Ferreira, F.Y. Liew, and F.Q. Cunha. 2009. Prostaglandin mediates IL-23/IL-17-induced neutrophil migration in inflammation by inhibiting IL-12 and IFNgamma production. *Proc Natl Acad Sci U S A* 106:5954-5959.

Levin, M., M.J. Newport, S. D'Souza, P. Kalabalikis, I.N. Brown, H.M. Lenicker, P.V. Agius, E.G. Davies, A. Thrasher, N. Klein, and et al. 1995. Familial disseminated atypical mycobacterial infection in childhood: a human mycobacterial susceptibility gene? *Lancet* 345:79-83.

Love, M.I., C. Soneson, P.F. Hickey, L.K. Johnson, N.T. Pierce, L. Shepherd, M. Morgan, and R. Patro. 2020. Tximeta: Reference sequence checksums for provenance identification in RNA-seq. *PLoS Comput Biol* 16:e1007664.

Lovewell, R.R., C.E. Baer, B.B. Mishra, C.M. Smith, and C.M. Sassetti. 2021. Granulocytes act as a niche for Mycobacterium tuberculosis growth. *Mucosal Immunol* 14:229-241.

Lowe, D.M., A.K. Bandara, G.E. Packe, R.D. Barker, R.J. Wilkinson, C.J. Griffiths, and A.R. Martineau. 2013. Neutrophilia independently predicts death in tuberculosis. *Eur Respir J* 42:1752-1757.

Lowe, D.M., J. Demaret, N. Bangani, J.K. Nakiwala, R. Goliath, K.A. Wilkinson, R.J. Wilkinson, and A.R. Martineau. 2018. Differential Effect of Viable Versus Necrotic Neutrophils on Mycobacterium tuberculosis Growth and Cytokine Induction in Whole Blood. *Front Immunol* 9:903.

910 Mahdaviani, S.A., M. Fallahi, M. Jamee, M. Marjani, P. Tabarsi, A. Moniri, P. Farnia, Z.
911 Daneshmandi, N. Parvaneh, J.L. Casanova, J. Bustamante, D. Mansouri, and A.A.
912 Velayati. 2022. Effective anti-mycobacterial treatment for BCG disease in patients
913 with Mendelian Susceptibility to Mycobacterial Disease (MSMD): a case series. *Ann*
914 *Clin Microbiol Antimicrob* 21:8.
915 Maloney, C.G., W.A. Kutchera, K.H. Albertine, T.M. McIntyre, S.M. Prescott, and G.A.
916 Zimmerman. 1998. Inflammatory agonists induce cyclooxygenase type 2 expression
917 by human neutrophils. *J Immunol* 160:1402-1410.
918 Martineau, A.R., S.M. Newton, K.A. Wilkinson, B. Kampmann, B.M. Hall, N. Nawroly, G.E.
919 Packe, R.N. Davidson, C.J. Griffiths, and R.J. Wilkinson. 2007. Neutrophil-mediated
920 innate immune resistance to mycobacteria. *J Clin Invest* 117:1988-1994.
921 Mills, K.H.G. 2023. IL-17 and IL-17-producing cells in protection versus pathology. *Nat Rev*
922 *Immunol* 23:38-54.
923 Mishra, B.B., R.R. Lovewell, A.J. Olive, G. Zhang, W. Wang, E. Eugenin, C.M. Smith, J.Y.
924 Phuah, J.E. Long, M.L. Dubuke, S.G. Palace, J.D. Goguen, R.E. Baker, S. Nambi, R.
925 Mishra, M.G. Booty, C.E. Baer, S.A. Shaffer, V. Dartois, B.A. McCormick, X. Chen, and
926 C.M. Sassetti. 2017. Nitric oxide prevents a pathogen-permissive granulocytic
927 inflammation during tuberculosis. *Nat Microbiol* 2:17072.
928 Moorlag, S., Y.A. Rodriguez-Rosales, J. Gillard, S. Fanucchi, K. Theunissen, B. Novakovic, C.M.
929 de Bont, Y. Negishi, E.T. Fok, L. Kalafati, P. Verginis, V.P. Mourits, V. Koeken, L.C.J. de
930 Bree, G.J.M. Pruijn, C. Fenwick, R. van Crevel, L.A.B. Joosten, I. Joosten, H. Koenen,
931 M.M. Mhlanga, D.A. Diavatopoulos, T. Chavakis, and M.G. Netea. 2020. BCG
932 Vaccination Induces Long-Term Functional Reprogramming of Human Neutrophils.
933 *Cell Rep* 33:108387.
934 Morgan, M., V. Obenchain, J. Hester, and H. Pagès. 2018. SummarizedExperiment:
935 SummarizedExperiment container. In.
936 Nandi, B., and S.M. Behar. 2011. Regulation of neutrophils by interferon-gamma limits lung
937 inflammation during tuberculosis infection. *The Journal of experimental medicine*
938 208:2251-2262.
939 Napolitani, G., E.V. Acosta-Rodriguez, A. Lanzavecchia, and F. Sallusto. 2009. Prostaglandin
940 E2 enhances Th17 responses via modulation of IL-17 and IFN-gamma production by
941 memory CD4+ T cells. *Eur J Immunol* 39:1301-1312.
942 Nwongbouwoh Muefong, C., O. Owolabi, S. Donkor, S. Charalambous, A. Bakuli, A. Rachow,
943 C. Geldmacher, and J.S. Sutherland. 2022. Neutrophils Contribute to Severity of
944 Tuberculosis Pathology and Recovery From Lung Damage Pre- and Posttreatment.
945 *Clin Infect Dis* 74:1757-1766.
946 Pai, M., M.A. Behr, D. Dowdy, K. Dheda, M. Divangahi, C.C. Boehme, A. Ginsberg, S.
947 Swaminathan, M. Spigelman, H. Getahun, D. Menzies, and M. Raviglione. 2016.
948 Tuberculosis. *Nat Rev Dis Primers* 2:16076.
949 Patro, R., G. Duggal, M.I. Love, R.A. Irizarry, and C. Kingsford. 2017. Salmon provides fast and
950 bias-aware quantification of transcript expression. *Nat Methods* 14:417-419.
951 Pavan Kumar, N., K. Moideen, A. Nancy, V. Viswanathan, B.S. Shruthi, S. Shanmugam, S.
952 Hissar, H. Kornfeld, and S. Babu. 2019. Plasma Eicosanoid Levels in Tuberculosis and
953 Tuberculosis-Diabetes Co-morbidity Are Associated With Lung Pathology and
954 Bacterial Burden. *Front Cell Infect Microbiol* 9:335.

955 Pearl, J.E., B. Saunders, S. Ehlers, I.M. Orme, and A.M. Cooper. 2001. Inflammation and
956 lymphocyte activation during mycobacterial infection in the interferon-gamma-
957 deficient mouse. *Cell Immunol* 211:43-50.
958 Peres, C.M., L. de Paula, A.I. Medeiros, C.A. Sorgi, E.G. Soares, D. Carlos, M. Peters-Golden,
959 C.L. Silva, and L.H. Faccioli. 2007. Inhibition of leukotriene biosynthesis abrogates the
960 host control of Mycobacterium tuberculosis. *Microbes Infect* 9:483-489.
961 Ramakrishnan, L. 2012. Revisiting the role of the granuloma in tuberculosis. *Nat Rev*
962 *Immunol* 12:352-366.
963 Rockwood, N., E. du Bruyn, T. Morris, and R.J. Wilkinson. 2016. Assessment of treatment
964 response in tuberculosis. *Expert Rev Respir Med* 10:643-654.
965 Sadikot, R.T., H. Zeng, A.C. Azim, M. Joo, S.K. Dey, R.M. Breyer, R.S. Peebles, T.S. Blackwell,
966 and J.W. Christman. 2007. Bacterial clearance of Pseudomonas aeruginosa is
967 enhanced by the inhibition of COX-2. *Eur J Immunol* 37:1001-1009.
968 Serezani, C.H., J. Chung, M.N. Ballinger, B.B. Moore, D.M. Aronoff, and M. Peters-Golden.
969 2007. Prostaglandin E2 suppresses bacterial killing in alveolar macrophages by
970 inhibiting NADPH oxidase. *Am J Respir Cell Mol Biol* 37:562-570.
971 Sheppe, A.E.F., and M.J. Edelmann. 2021. Roles of Eicosanoids in Regulating Inflammation
972 and Neutrophil Migration as an Innate Host Response to Bacterial Infections. *Infect*
973 *Immun* 89:e0009521.
974 Silva, M.T., M.N. Silva, and R. Appelberg. 1989. Neutrophil-macrophage cooperation in the
975 host defence against mycobacterial infections. *Microb Pathog* 6:369-380.
976 Soares, A.P., C.K. Kwong Chung, T. Choice, E.J. Hughes, G. Jacobs, E.J. van Rensburg, G.
977 Khomba, M. de Kock, L. Lerumo, L. Makhethe, M.H. Maneli, B. Pienaar, E. Smit, N.G.
978 Tena-Coki, L. van Wyk, W.H. Boom, G. Kaplan, T.J. Scriba, and W.A. Hanekom. 2013.
979 Longitudinal changes in CD4(+) T-cell memory responses induced by BCG vaccination
980 of newborns. *J Infect Dis* 207:1084-1094.
981 Souto, F.O., J.C. Alves-Filho, W.M. Turato, M. Auxiliadora-Martins, A. Basile-Filho, and F.Q.
982 Cunha. 2011. Essential role of CCR2 in neutrophil tissue infiltration and multiple
983 organ dysfunction in sepsis. *Am J Respir Crit Care Med* 183:234-242.
984 Tan, Z., R. Jiang, X. Wang, Y. Wang, L. Lu, Q. Liu, S.G. Zheng, B. Sun, and B. Ryffel. 2013.
985 RORgammat+IL-17+ neutrophils play a critical role in hepatic ischemia-reperfusion
986 injury. *J Mol Cell Biol* 5:143-146.
987 Taylor, P.R., S. Roy, S.M. Leal, Jr., Y. Sun, S.J. Howell, B.A. Cobb, X. Li, and E. Pearlman. 2014.
988 Activation of neutrophils by autocrine IL-17A-IL-17RC interactions during fungal
989 infection is regulated by IL-6, IL-23, RORgammat and dectin-2. *Nat Immunol* 15:143-
990 151.
991 Team, R.C. 2021. R: A Language and Environment for Statistical Computing. In Vienna,
992 Austria.
993 Thompson, E.G., Y. Du, S.T. Malherbe, S. Shankar, J. Braun, J. Valvo, K. Ronacher, G. Tromp,
994 D.L. Tabb, D. Alland, S. Shenai, L.E. Via, J. Warwick, A. Aderem, T.J. Scriba, J. Winter,
995 G. Walzl, D.E. Zak, and T.B.B.C. Catalysis. 2017. Host blood RNA signatures predict
996 the outcome of tuberculosis treatment. *Tuberculosis (Edinb)* 107:48-58.
997 Tobin, D.M., J.C. Vary, Jr., J.P. Ray, G.S. Walsh, S.J. Dunstan, N.D. Bang, D.A. Hagge, S.
998 Khadge, M.C. King, T.R. Hawn, C.B. Moens, and L. Ramakrishnan. 2010. The lta4h
999 locus modulates susceptibility to mycobacterial infection in zebrafish and humans.
1000 *Cell* 140:717-730.

1001 Torrado, E., and A.M. Cooper. 2010. IL-17 and Th17 cells in tuberculosis. *Cytokine Growth*
1002 *Factor Rev* 21:455-462.
1003 Tsuda, Y., H. Takahashi, M. Kobayashi, T. Hanafusa, D.N. Herndon, and F. Suzuki. 2004. Three
1004 different neutrophil subsets exhibited in mice with different susceptibilities to
1005 infection by methicillin-resistant Staphylococcus aureus. *Immunity* 21:215-226.
1006 Wickham, H. 2016. ggplot2: Elegant Graphics for Data Analysis. In Springer-Verlag New York,
1007 ISBN: 978-3-319-24277-4.
1008 Wu, T., E. Hu, S. Xu, M. Chen, P. Guo, Z. Dai, T. Feng, L. Zhou, W. Tang, L. Zhan, F. xiaochong,
1009 S. Liu, X. Bo, and G. Yu. 2021. clusterProfiler 4.0: A universal enrichment tool for
1010 interpreting omics data. *The Innovation* 2:100141-100141.
1011 Zhu, A., A. Srivastava, J.G. Ibrahim, R. Patro, and M.I. Love. 2019. Nonparametric expression
1012 analysis using inferential replicate counts. *Nucleic Acids Res* 47:e105.
1013

Figures and figure Legends:

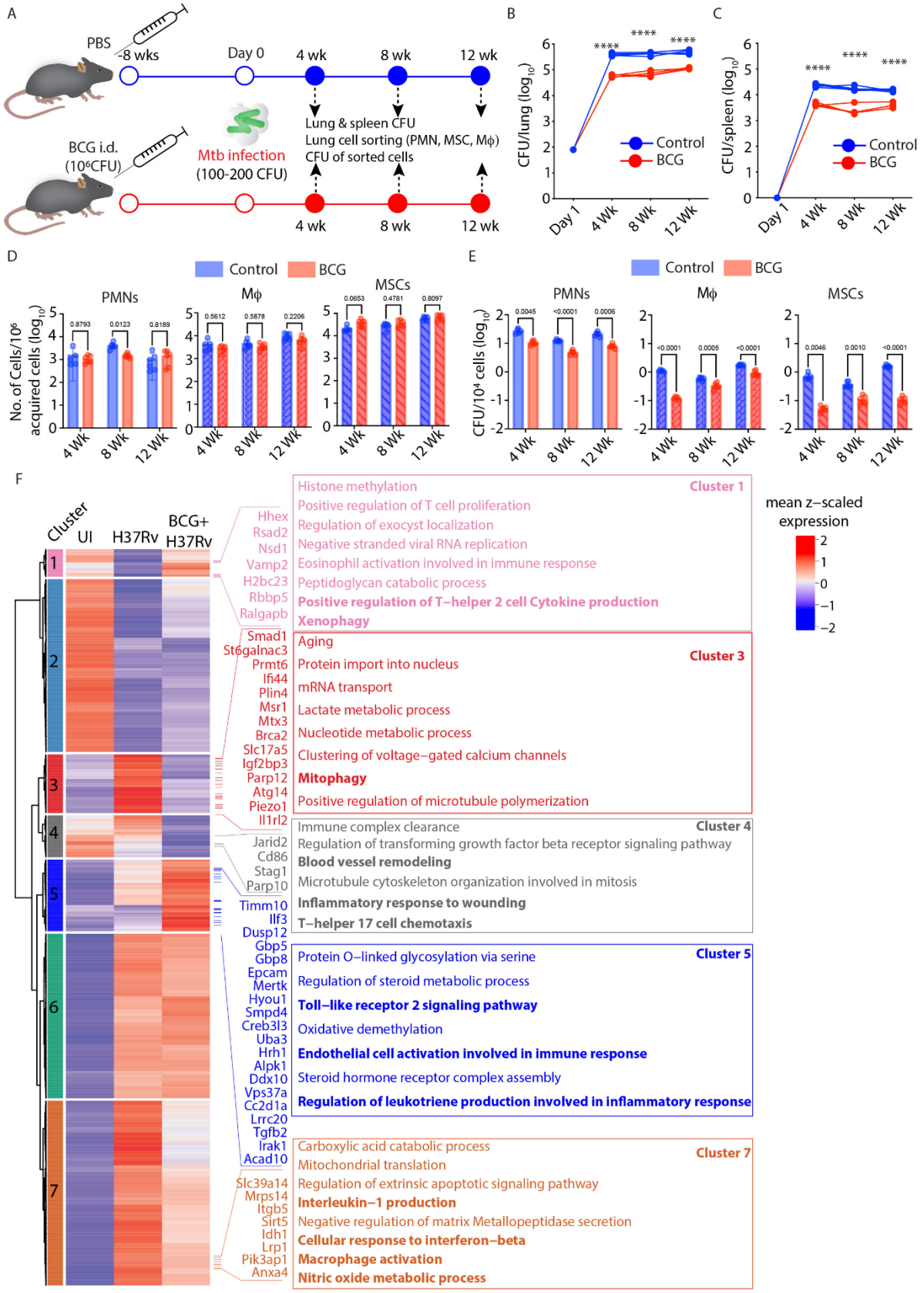

Figure 1: PMNs harbours substantial amount of *Mtb* and provide an immune-privileged niche to *Mtb*.

1019 (A) Study design for BCG vaccination experiment. C57BL/6 mice were vaccinated
1020 intradermally with 10^6 BCG bacilli, followed by aerosol infection with H37Rv (100-200
1021 CFU) 8 weeks post BCG vaccination. At 4,8,12 weeks post-infection, mice were euthanized
1022 for various studies. Time course of the lung (B) and spleen (C) bacterial burden in
1023 unvaccinated and BCG vaccinated groups (unpaired student's t-test was applied to compare
1024 both experimental groups at different time points. (D) Quantification of the sorted cells
1025 normalized to per 1 million of total acquired cells from the lungs of vaccinated and
1026 unvaccinated mice. (E) Determination of *Mtb* burden in individual sorted cells, plotted as
1027 CFU/10^4 sorted cells at 4,8,12 weeks post-infection, from the lungs of vaccinated and
1028 unvaccinated mice. Experimental groups were evaluated using a 2-way ANOVA statistical
1029 test. n= 5 mice/group in all treatment groups. (F) Heatmap of DEGs representing the z-scaled
1030 normalised average expression in each group. The DEGs are clustered using Euclidean
1031 distance and ward D2 methodology. Each cluster reflects significantly enriched GO BP terms
1032 unique to the cluster.
1033

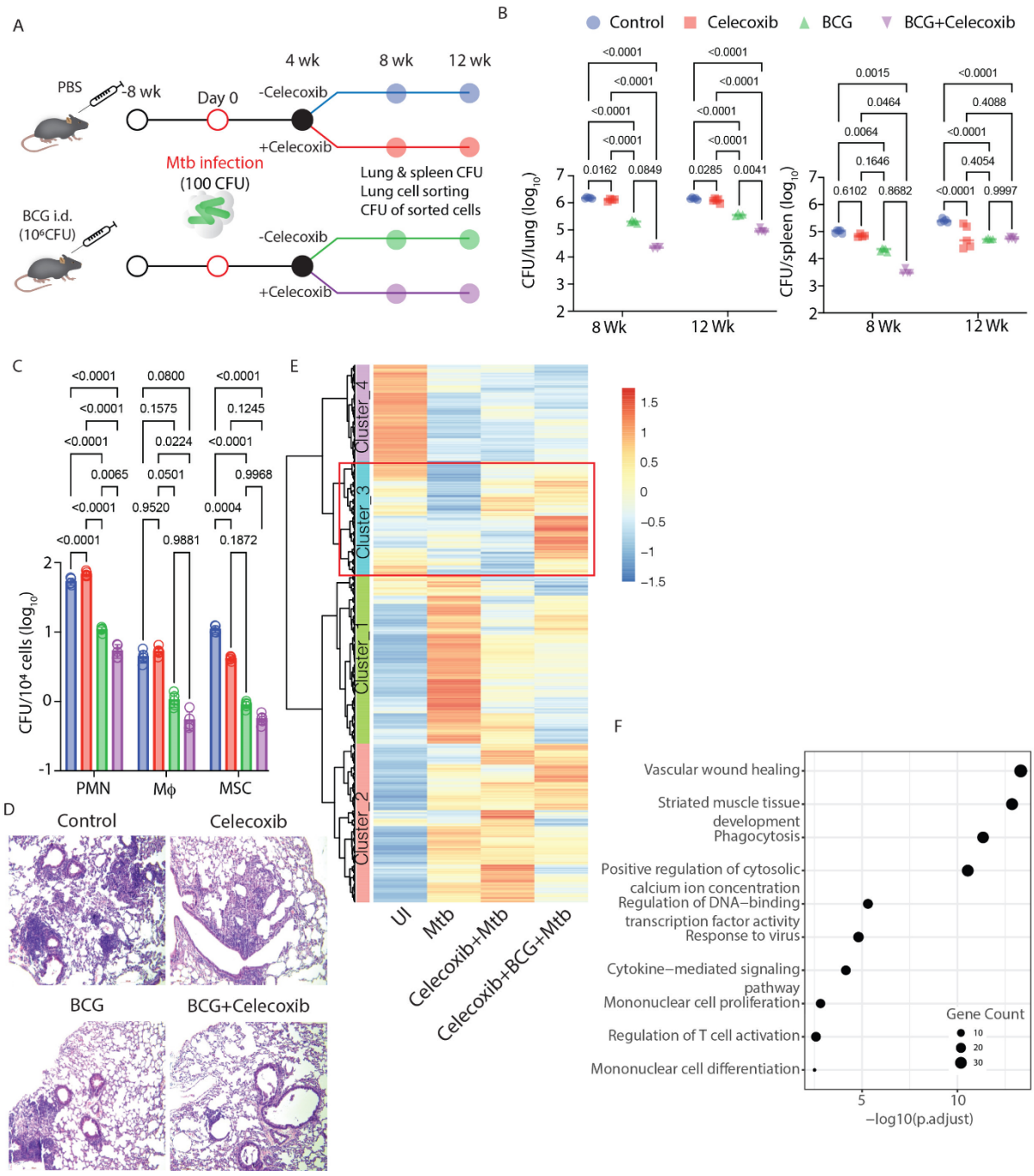

Figure 2: PMN-resident *Mtb* in BCG-vaccinated mice is susceptible to celecoxib treatment.

(A) Study plan. C57BL/6 mice were vaccinated intradermally with 10^6 BCG bacilli. After 8 weeks, vaccinated and unvaccinated mice were subjected to aerosol infection with H37Rv (100 CFU). 4 weeks post *Mtb* infection, mice received celecoxib (50mg/kg, orally) treatment for 4 and 8 weeks in with and without BCG vaccination group keeping the untreated arm as control. At 4,8,12 weeks post-infection, mice were euthanized, and lung and spleen were harvested. (B) Enumeration of lung and spleen bacterial burden in all four treatment groups (Control, BCG-vaccinated, celecoxib-treated and BCG-vaccinated celecoxib-treated) at 8- and 12-weeks post-infection. (C) *Mtb* burden in individual sorted cells (PMNs, Macrophages and MSCs), plotted as CFU/10^4 sorted cells at 12 weeks post-infection time point, from the lungs of all 4 treatment groups of mice. A 2-way ANOVA statistical test was applied to compare all 4 treatment groups at different time points. Sample size (n) = 5 mice/group in all

1048 treatment groups. (D) H&E-stained lung sections of Control, BCG-vaccinated, celecoxib-
1049 treated and BCG-vaccinated celecoxib-treated group at 10X magnification. (E) The average
1050 z-scaled expression of the DEGs identified between each pairwise comparison is represented
1051 in the heatmap. The data for UI and *Mtb* groups are the same as used in Fig. 1F, being part of
1052 the common RNAseq experiment. (F) Significantly enrichment GO BP (p-adjusted ≤ 0.1)
1053 highlights immune response against pathogens from the DEGs set of cluster 3.
1054

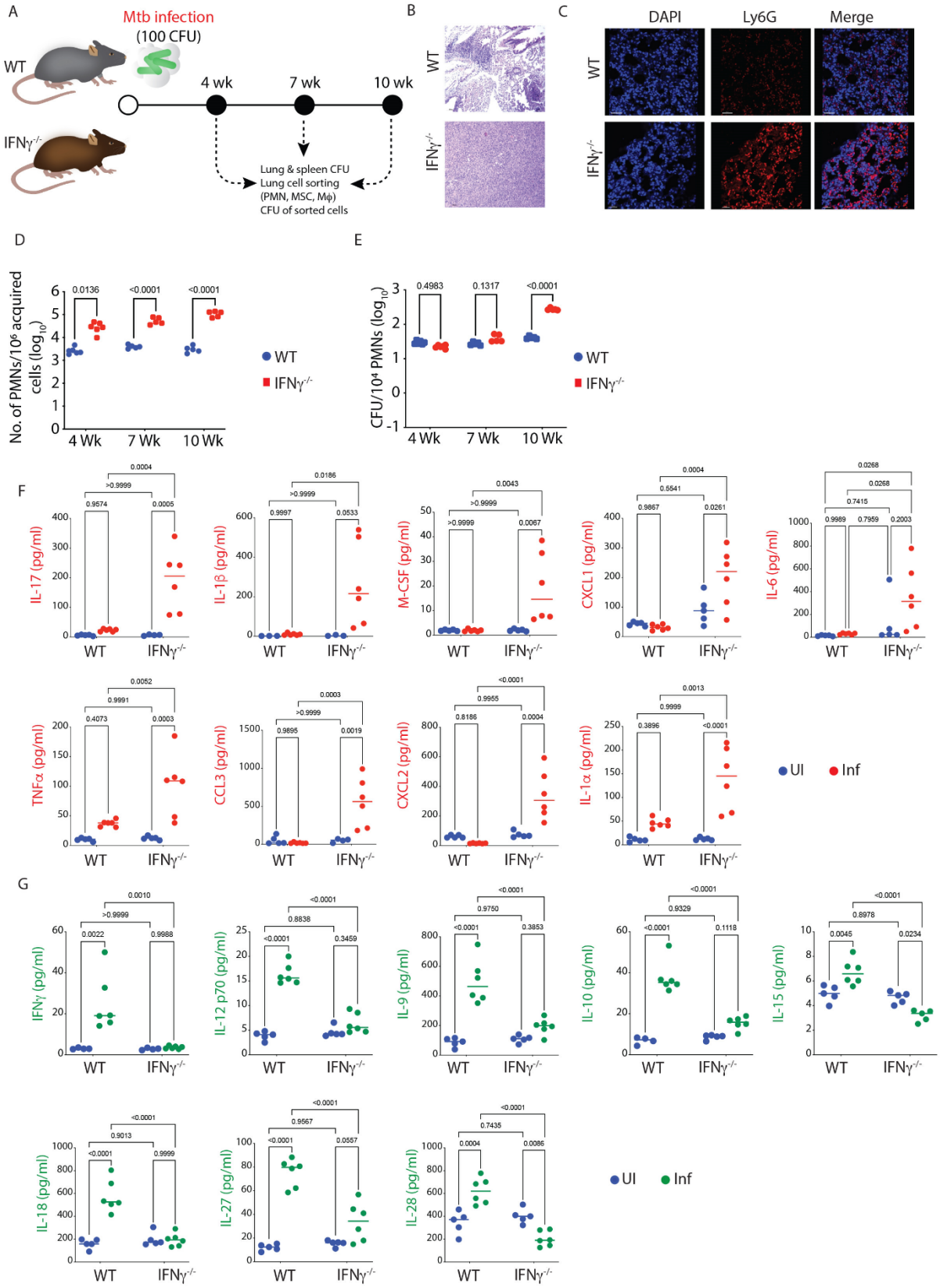

Figure 3: Loss of IFNγ leads to uncontrolled neutrophilia, huge *Mtb* burden, severe disease pathology and death.

(A) Experimental design and timeline. C57BL/6 mice (WT and *IFNγ*$^{-/-}$) were infected with H37Rv, 100 CFU, via the aerosol route. Mice from both groups were euthanized at 4,7- and 10 weeks post-infection time-point. Lung and spleen tissues were harvested and processed for

diverse assays, as shown in the study design. (B) H&E-stained lung sections of WT and *IFNγ* $^{-/-}$ mice at 10X magnification, showing severe histopathology in the latter group of mice. (C) Lung IFA images from the same group of mice showing the extensive infiltration of PMNs (Ly6G^{+} cells stained in red colour) in *Mtb*-infected *IFNγ* $^{-/-}$ mice compared to WT mice. (D) Number of PMNs in the lungs of *Mtb* infected WT and *IFNγ* $^{-/-}$, normalized to per 1 million of total acquired cells, at 4,7- and 10 weeks post infection timepoint. (E) *Mtb* burden in the PMNs, sorted from the lung of *Mtb* infected WT and *IFNγ* $^{-/-}$ (plotted as CFU/10^{4} sorted cells) at 4,7- and 10 weeks post-infection. Experimental groups were evaluated using a 2-way ANOVA statistical test. Sample size (n)= 5-6 mice/group in all treatment groups. Luminex data: Quantification of several cytokines and chemokines from the lung supernatant of uninfected and *Mtb*-infected WT and *IFNγ* $^{-/-}$ mice. (F) Cytokines and chemokines that are upregulated in *Mtb*-infected *IFNγ* $^{-/-}$ mice compared to WT mice (G) Cytokines and chemokines that are downregulated in *Mtb*-infected *IFNγ* $^{-/-}$ mice compared to WT mice. Data was evaluated using a 2-way ANOVA statistical test. Sample size (n)= 5-6 mice/group in all treatment groups.

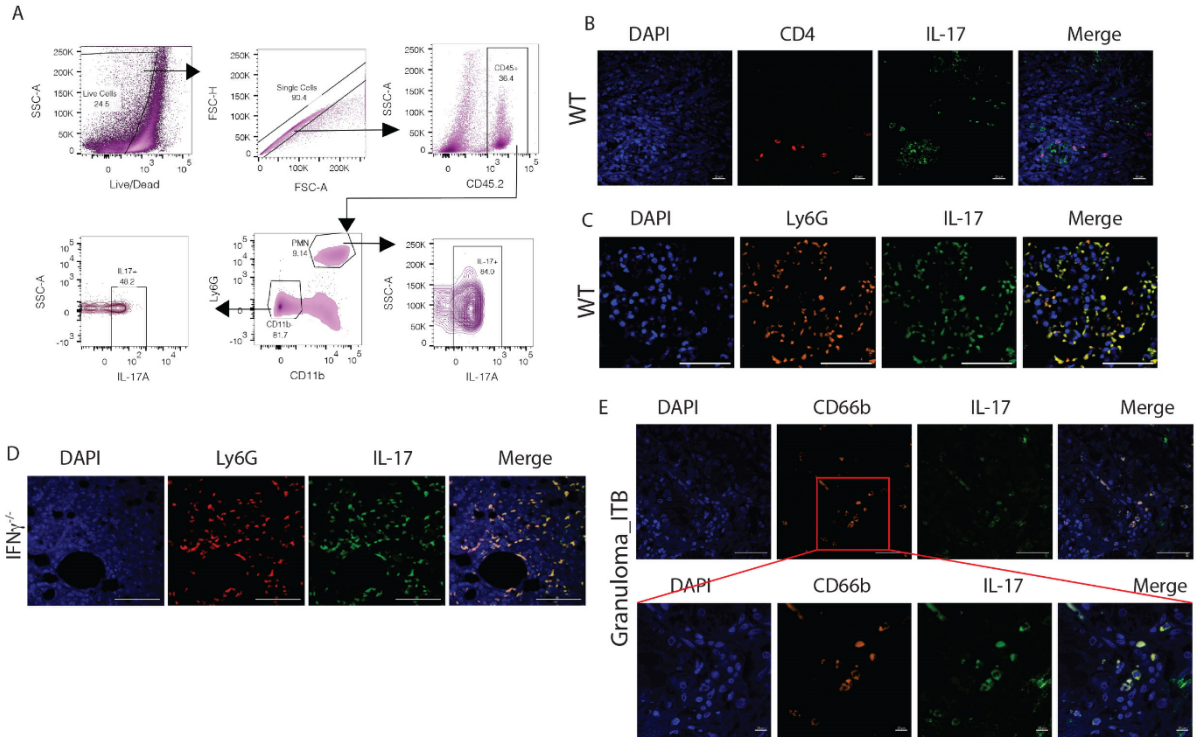

Figure 4: PMNs are one of the major sources of IL-17 in the lungs of *Mtb*-infected mice. (A) Lung cells from WT *Mtb*-infected mice were stained with different antibodies and were assayed through flow cytometry to elucidate the cellular source for elevated IL-17. FACS gating strategy showing PMNs (Ly6G^{+} CD11b^{+} cells)) as the dominant producer of IL-17 in the lungs of *Mtb*-infected mice compared to Ly6G^{-} CD11b^{-} cells. (B) IFA images of the lungs of *Mtb*-infected WT mice at 6 weeks post-infection time-point showing the co-localization of CD4^{+} T cells (shown in red colour) and IL-17 (shown in green colour). IFA images of the lungs of *Mtb*-infected WT (C) and *IFNγ* $^{-/-}$ (D) mice at 6 weeks post-infection time-point showing the co-localization of PMNs (Ly6G^{+} cells shown in red colour) and IL-17 (shown in green colour). (E) Co-localization of PMNs (CD66b^{+} cells shown in red colour) and IL-17 (shown in green colour) in the gut granuloma sections of intestinal TB (ITB) patients.

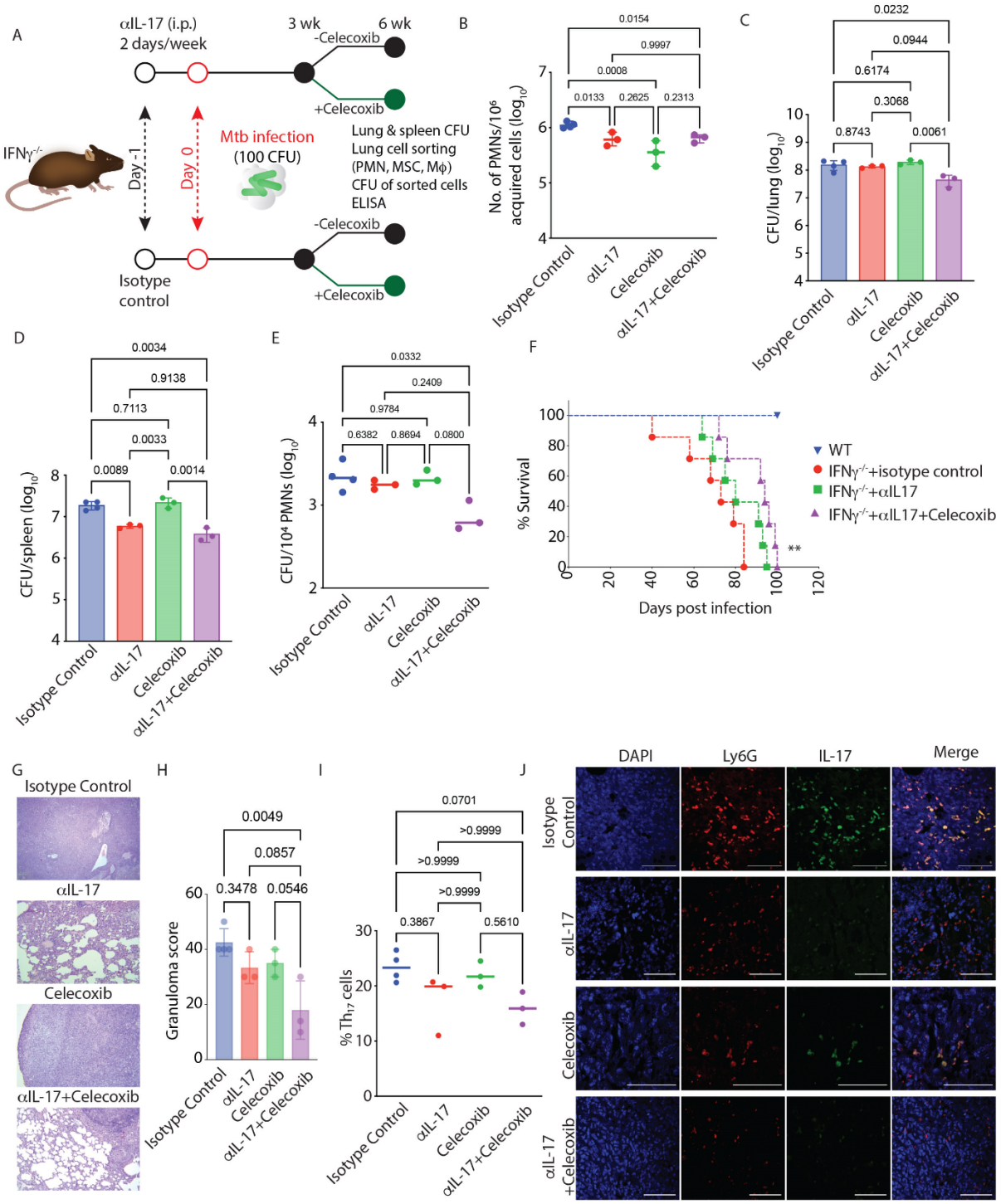

Figure 5: Celecoxib treatment with IL-17 neutralization reverses IL-17-dependent neutrophilia and controls TB disease in *IFNγ*$^{-/-}$ mice.

(A) Study plan. *IFNγ*$^{-/-}$C57BL/6 mice infected with H37Rv at a dose of 100 CFU via the aerosol route. One arm of the *Mtb*-infected mice received an αIL-17 neutralizing antibody (100µg/mouse), and the other arm received an isotype control antibody (100µg/mouse) intraperitoneally twice in a week, starting a day before *Mtb* infection. After 3 weeks of infection, both the groups of mice were further divided into two groups, one that received celecoxib (50mg/kg, orally) for 3 weeks and the other that received vehicle control (DMSO here). Mice from all four groups of mice were euthanized at 6 weeks post *Mtb* infection, and their lungs and spleen were harvested, and serum was stored for ELISA. (B) PMN's count,

1102 normalized to 1 million total acquired cells, in the lungs of infected mice in all four treatment
1103 groups at 6 weeks post-infection. Bacterial burden in lungs (C) and spleen (D) of *Mtb*
1104 infected mice from described treatment groups at 6 weeks post-infection time-point sacrifice.
1105 (E) CFU (normalized to per 10^4 sorted cells) inside PMNs sorted out from the lungs of
1106 infected mice at 6 weeks post-infection sacrifice. (n= 3-4 mice/group). The statistical
1107 significance of the treatment groups was assessed by applying a one-way ANOVA test. (F)
1108 Survival curve of the group of *Mtb* infected *IFNγ*$^{-/-}$ mice that received αIL-17 neutralizing
1109 antibody, celecoxib alone or together, along with the untreated control group and infected
1110 WT mice group. Both mice strains were infected with 100 CFU of H37Rv through an aerosol
1111 route. One arm of the *Mtb*-infected mice received an αIL-17 neutralizing antibody, and the
1112 other arm received an isotype control antibody twice a week, starting a day before the *Mtb*
1113 infection. After 3 weeks of infection, both the groups of mice were further divided into two
1114 groups, one that received celecoxib for 3 weeks and the other that received vehicle control
1115 (DMSO). Mice were incubated till their natural death. The time of death of each mouse was
1116 noted and plotted for survival analysis (n= 7 mice/group). (G) H&E-stained lung sections
1117 showing pathology in the αIL-17Ab+Celecoxib group. (H) Granuloma scoring for lung
1118 pathology from all 4 treatment groups. (I) %Th_{17} cells (gated on CD4 T cells) in the lungs of
1119 mice from the same treatment groups described above. (J) Lung IFA images from the above-
1120 stated treated group of mice show the colocalization (yellow) of PMNs ($Ly6G^+$ cells shown in
1121 red colour) and IL17 (shown in green colour).
1122

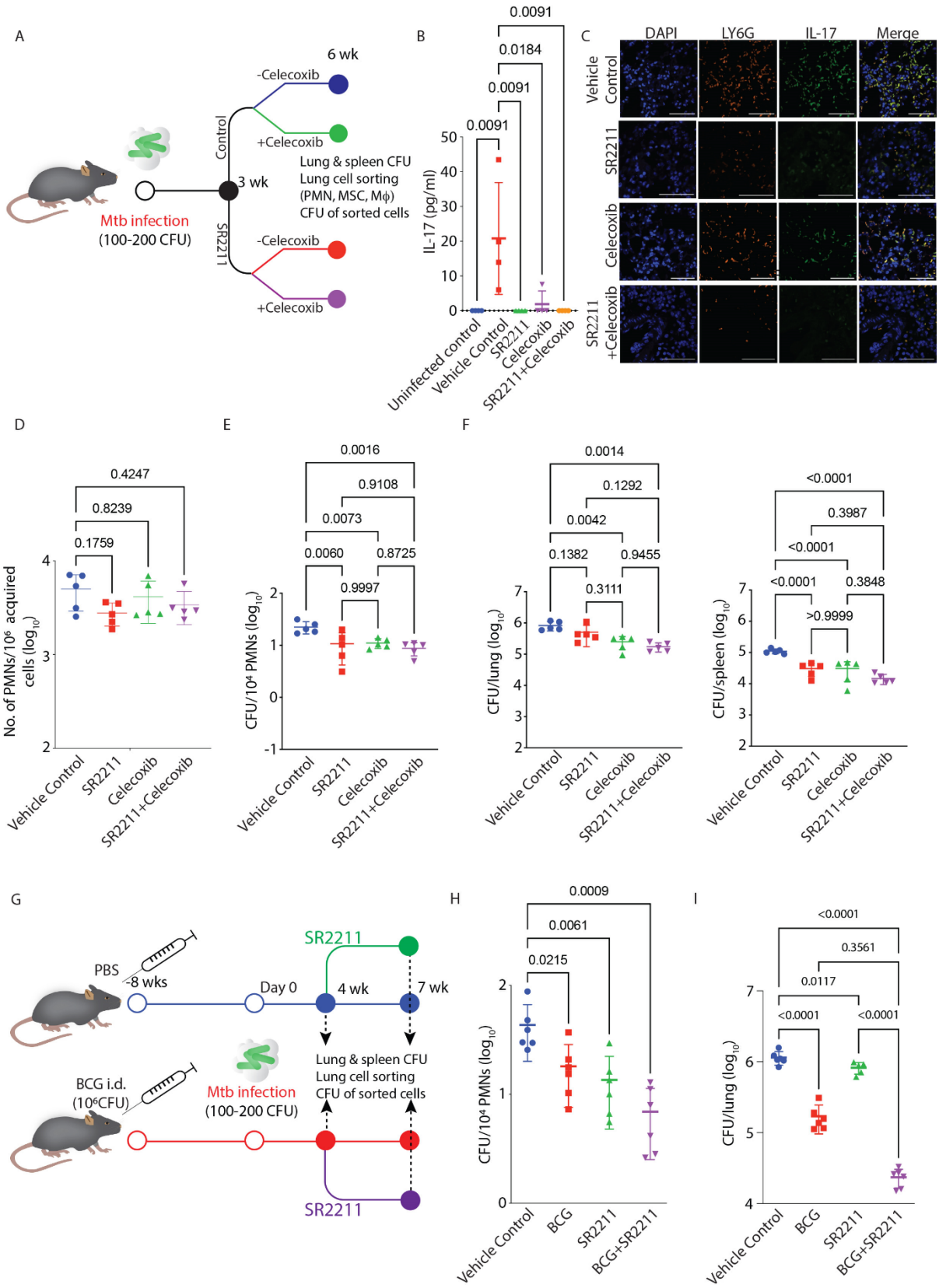

Figure 6: RORγt inhibition brings down *Mtb* burden and augments BCG vaccine efficacy in WT mice.

(A) Study plan. C57BL/6 mice were infected with H37Rv at a 100-200 CFU dose via the aerosol route. At 3 weeks post-infection, treatment with celecoxib and SR 2211 (inverse agonist for RORγt) was started for further 3 weeks. Celecoxib (50mg/kg) was administered

orally once a day, and SR 2211 (20mg/kg) was administered intraperitoneally thrice in a week. At 6 weeks post-infection, mice from the treatment and untreated control groups were sacrificed, lung and spleen were harvested for CFU, histopathology and FACS analysis, and lung homogenates were stored for ELISA. (B) Levels of IL-17 in the lung homogenates of all four-treatment groups of mice. (C) Lung IFA images from the above-stated treated group of mice show the colocalization (yellow) of PMNs ($Ly6G^+$ cells shown in red colour) and IL17 (shown in green colour). (D) Lung PMN's count normalized to 1 million of total acquired cells, (E) Lung PMN's *Mtb* burden normalized to per 10^4 sorted cells, (F) mycobacterial burden in lung and spleen, in the above-stated treatment groups of mice. The statistical significance of the treatment groups was assessed by applying a one-way ANOVA test, n=5 mice/group. (G) Experimental plan. C57BL/6 mice were vaccinated intradermally with 10^6 BCG bacilli for 8 weeks, followed by aerosol infection with H37Rv at a dose of 100-200 CFU. 4 weeks post-infection, treatment with SR2211 was started for additional 3 weeks, intraperitoneally, thrice a week. At 7 weeks post-infection, mice from the described four treatment groups were sacrificed, and lung and spleen were harvested for CFU and FACS analysis. (H) CFU (normalized to per 10^4 sorted cells) inside PMNs sorted from the lungs of infected mice at 7 weeks post-infection time-point. (I) *Mtb* burden in the lungs of infected mice at 7 weeks post-infection (n= 5-6 mice/group). The statistical significance of the treatment groups was assessed by applying a one-way ANOVA test.

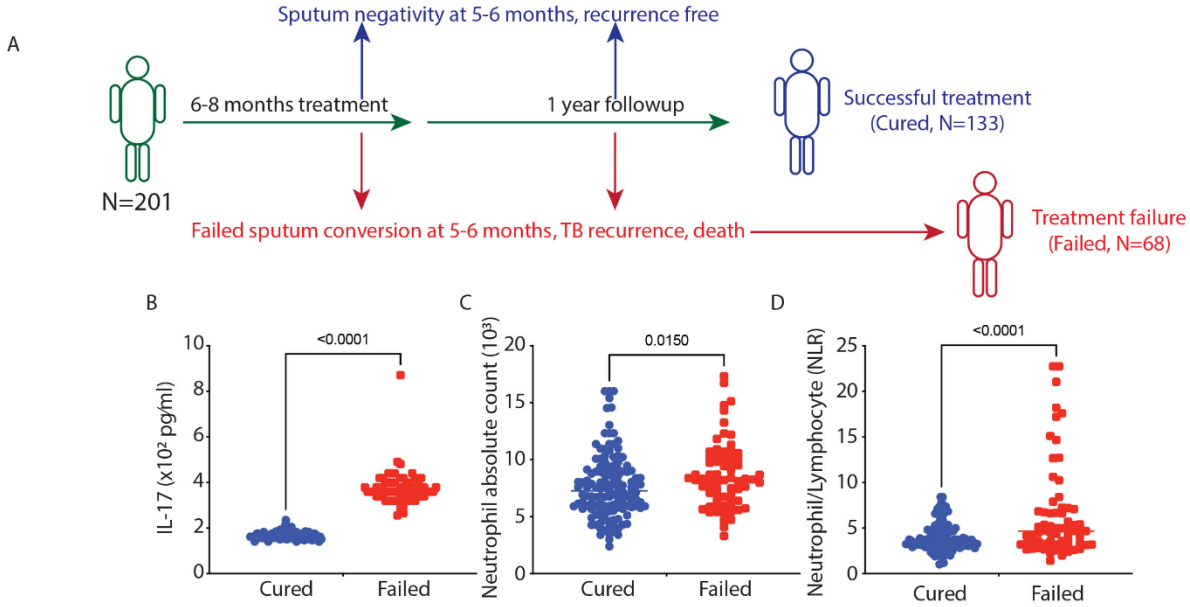

Figure 7: High IL-17 precipitates adverse treatment outcomes in pulmonary TB patients.

(A) Pulmonary TB (PTB) patients-cohort study design: It includes 133 subjects that were cured of TB after the full standard ATT regime and 68 subjects that have failed the standard ATT regime (independent of drug resistance) or have experienced recurrence of symptoms. At the time of recruitment in the cohort study, the baseline blood levels of IL17, neutrophils, total lymphocytes in both the treatment groups were measured. (B) blood IL17 levels, (C) blood neutrophils level and (D) blood neutrophil/total lymphocyte ratio in treatment failure and treatment success cases of pulmonary TB patients. Unpaired t-test was applied to calculate significance.